Chemical Science

ROYAL SOCIETY OF CHEMISTRY

REVIEW

View Article Online
View Journal | View Issue

Cite this: *Chem. Sci.*, 2025, **16**, 18005

Recent advances in interface engineering for photoelectrochemical detection of new pollutants

Xiaoyu Dong,†[a] Wenhong Yang,†[b] Liuyong Hu,*[a] Wenling Gu*[b] and Chengzhou Zhu *[b]

Photoelectrochemical (PEC) sensing has become a hot research topic due to its low cost and ideal sensitivity and has received widespread attention. However, the inherent complexity of multiple charge separation, transfer, and recombination pathways poses a major challenge. Inefficient charge separation, rapid recombination, and sluggish interfacial reactions of photogenerated carriers collectively limit photoelectric performance and compromise long-term operational stability. Moreover, conventional surface functionalization with insulating biorecognition macromolecules—commonly used to enhance specificity—often leads to reduced sensitivity due to suppressed charge transfer. These limitations underscore the urgent need for advanced surface and interface engineering strategies to improve PEC sensing efficiency and stability. We have provided a comprehensive overview of the latest developments in PEC interface engineering, with a focus on three key aspects: transfer channel, interface catalysis, and interface recognition. Significant research milestones in the detection of new pollutants using engineered PEC interfaces are highlighted. Through critical analysis and comparative discussion, we evaluate the advantages and limitations of various interface design strategies. Finally, we outline future directions and opportunities for developing next-generation PEC sensors with enhanced performance, emphasizing the pivotal role of rational interface engineering in achieving efficient, selective, and durable PEC sensing platforms.

Received 13th August 2025
Accepted 10th September 2025

DOI: 10.1039/d5sc06181d

rsc.li/chemical-science

1 Introduction

Photoelectrochemical (PEC) sensing has become a powerful platform for rapid and accurate detection of chemical and biochemical molecules, leveraging its advantages of operational simplicity, short response times, high sensitivity, and low cost.[1,2] The PEC process involves the mutual conversion of electrical and chemical energy. Electron–hole pairs are generated when photons exceeding the bandgap energy of photoactive materials are irradiated, which then migrate to the electrode interface to participate in redox reactions.[3] In PEC sensing systems, signal transducers are composed of photosensitive materials fixed on the surface of electrodes, modulating photoelectric responses in direct correlation with target-specific interactions.[4,5] This interplay, including photophysical mechanisms and interfacial redox chemistry, supports the versatility of PEC platforms, not only for fundamental mechanism investigations but also for the development of highly sensitive analytical tools applicable across environmental monitoring, biomedical diagnostics, and energy-related research.[6–12]

Advanced interface engineering has become the key to meeting high-performance PEC sensing requirements.[13,14] As mentioned above, the three key steps in the photoelectric conversion process are photoexcitation, separation and migration of electron–hole pairs generated by light towards the surface, and surface redox interactions. To improve the photoelectric efficiency, one or more of the above three processes can be improved as a practical strategy. Specifically, the performance of PEC sensors is intrinsically limited by the light absorption efficiency and charge separation kinetics of their photoactive components.[15,16] Moreover, another persistent challenge lies in sluggish interfacial reactions, which accelerate material corrosion and degrade long-term operational stability.[17,18] Recent advances in interfacial engineering aim to address these limitations by optimizing carrier transport pathways and integrating cocatalysts to establish efficient charge transfer channels. In addition, conventional surface modifications employing insulating biorecognition macromolecules often compromise photoelectric responses, weakening the detection sensitivity.[19–26] At this time, emerging approaches

[a]*Hubei Key Laboratory of Plasma Chemistry and Advanced Materials, Hubei Engineering Technology Research Center of Optoelectronic and New Energy Materials, Wuhan Institute of Technology, Wuhan 430205, P. R. China. E-mail: huly@wit.edu.cn*

[b]*State Key Laboratory of Green Pesticide, International Joint Research Center for Intelligent Biosensing Technology and Health, College of Chemistry, Central China Normal University, Wuhan 430079, P. R. China. E-mail: wlgu@ccnu.edu.cn; czzhu@ccnu.edu.cn*

† These authors contributed equally (Xiaoyu Dong and Wenhong Yang).

leverage molecularly engineered recognition units and dynamically adaptive interfacial design to achieve precise detection.[27,28] Therefore, efficient interface engineering is expected to meet high-performance PEC sensing requirements.

At present, some new methods for interface engineering have been developed to improve the above mentioned problems, thereby achieving interface regulation to enhance PEC sensing. However, recent reviews regarding PEC sensing mainly focus on signal amplification strategies by using an enzyme-catalyzed reaction,[29] nucleic acid cycle amplification[30] and redox cascade reaction.[31] Furthermore, advances in the PEC sensing mode regulation have also been summarized, involving signal-off mode,[32] signal-on mode[33] and photocurrent polarity switching mode.[34] There are still no review articles focusing on interface engineering for boosting PEC sensing. These studies mostly focus on macroscopic performance optimization, while neglecting the underlying regulatory mechanisms by which the interface microstructure influences sensing performance. Actually, the sensitivity, selectivity, and stability of PEC sensors essentially depend on the interface behavior between the photoactive material and the analyte/electrolyte, including interface structure regulation, catalytic activity optimization, and the creation of novel sensing interfaces. Herein, we highlight the recent research efforts on interface engineering as a promising solution as well as the underlying mechanisms and challenges in PEC sensing applications (Fig. 1). New pollutants of widespread concern both domestically and internationally include persistent organic pollutants (POPs), antibiotics, microplastics and endocrine disruptors. To assess the environmental risk posed by new pollutants, we need to use relatively accurate and fast methods to identify them. By interface engineering, PEC sensors achieve excellent performance in aspects of catalytic activity, selectivity, and stability, establishing them as essential tools for real-time, on-site monitoring in new pollutant control and regulatory compliance. Finally, we conclude with some perspectives and challenges in the development of rational interface engineering for next-generation PEC sensors.

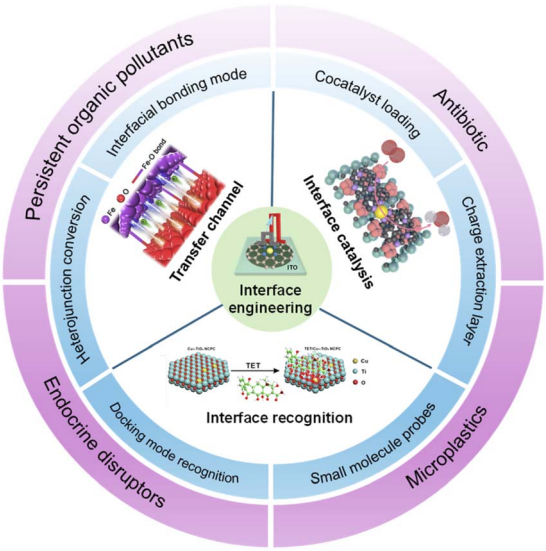

Fig. 1 Schematic diagram of various PEC interface regulation strategies for sensing applications.

2 PEC sensing mechanism

2.1 Photoelectric conversion process

We know that the photons absorbed by photoactive materials have sufficient energy to generate electron–hole pairs. When photons exceeding the bandgap energy of photoactive materials are irradiated, electron–hole pairs are generated and then migrate to the electrode interface to participate in redox reactions.[35] The widely accepted mechanism involves four sequential steps: (i) photon absorption; (ii) charge separation; (iii) charge migration and recombination; and (iv) charge utilization.[36] It is worth noting that the processes of charge separation and surface catalytic reactions are not independent, but rather synergistic. Generally, the light absorption efficiency (η_{abs}), the bulk phase separation efficiency (η_{sep}), and the surface injection efficiency (η_{inj}) mainly affect the performance of the photoelectrode, which can be expressed as $J = \eta_{abs} \times \eta_{sep} \times \eta_{inj}$.[37,38] Here, η_{abs} refers to photon absorption and exciton generation, η_{sep} refers to charge separation and transport to the interface, and η_{inj} refers to interfacial charge transfer efficiency. A more comprehensive understanding can be achieved by analyzing specific parameters that characterize the distinct roles of various materials within the photoelectrode.

2.2 Challenges in PEC sensing

The PEC process is highly intricate, involving light harvesting, charge separation, and catalytic reactions, each spanning a wide range of temporal and spatial scales. In particular, the charge separation process is characterized by its vast temporal span, linking ultrafast photoexcitation (within fs) to slower surface reactions (ms to s), while simultaneously requiring energy transfer within nanoscale spaces in Fig. 2.[39]

The interplay of multiple charge separation, transfer, and recombination pathways further increases the complexity. These complexities make the effective separation and transfer

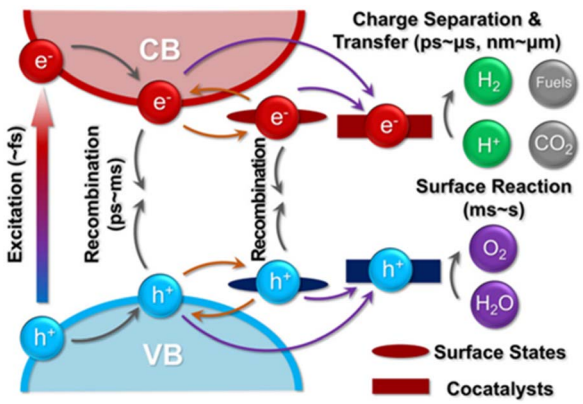

Fig. 2 A schematic depiction of the photocatalytic processes occurring across timescales from femtoseconds to seconds.[40] Copyright 2022, John Wiley and Sons.

of photogenerated charges a major challenge. During this process, the migration of photo-generated electrons and holes in divergent directions leads to differences in the surface potential of semiconductors, which can be evaluated by surface photovoltage (SPV) measurements. To elucidate the associated chemical states and band alignments under operational conditions, *in situ* X-ray photoelectron spectroscopy (XPS) serves as an effective tool to monitor surface redox processes and interfacial charge redistributions. Concurrently, transient photocurrent and photovoltage measurements emerge as effective methodologies to evaluate carrier separation efficiency, offering critical insights into the splitting of quasi-Fermi levels for both electrons and holes, as well as the kinetics of surface reactions. Femtosecond transient absorption spectroscopy (fs-TAS) is predominantly utilized to explore the transient relaxation process of electron–hole pairs within the excited states, typically exhibiting lifetimes in the picosecond regime. Conversely, time-resolved photoluminescence (TRPL) serves to investigate the radiative transitions as these excited states transition back to their ground states, revealing longer-lived phenomena generally observed on the nanosecond timescale. Moreover, Kelvin probe force microscopy (KPFM) and surface plasmon resonance spectroscopic visualization (SPRSV) enable direct mapping of charge carrier transfer and accumulation under operational conditions, facilitating the assessment of surface voltage differentials across crystal planes. Additionally, surface photoelectrochemical measurements (SPECMs) yield complementary data by monitoring capacitance, charge transfer resistance, and localized surface redox currents. Collectively, these methodologies enable a comprehensive analysis of charge carrier dynamics across both the bulk and surface regions of photocatalytic materials, advancing our understanding of the underlying mechanisms driving PEC efficiency.

Moreover, charge recombination occurs on ultrafast time scales (picoseconds to milliseconds) and competes strongly with charge separation processes. Furthermore, the ability of efficient surface catalytic reactions is ideal, as catalytic reactions occur at slower time scales (μs–ms) compared to charge generation (fs–ps) and separation (ps–μs), highlighting the importance of long-lived charges and surface reactions in promoting kinetics. Faster catalytic reactions will facilitate more excellent charge separation. However, due to the complexity of the structure of some biomolecules, the conventional surface modification of insulating biometric macromolecules will usually damage the photoelectric response and weaken the detection sensitivity. In addition, because some probes lack recognition groups, the selectivity of these probes to specific small molecules is still insufficient. Therefore, it remains a challenge to develop a highly sensitive and selective interface recognition method.[40,41] Meanwhile, the stability of the photoelectrode is also one of the main factors that need to be considered to meet practical application requirements. Consequently, a thorough understanding of how different interface engineering strategies influence device performance is essential for developing optimized approaches to PEC sensing. We will introduce recent advances in interface engineering of PEC sensing and explain several general strategies that may alleviate various obstacles involved in achieving efficient PEC sensing.

3 Interface engineering

The PEC process comprises three fundamental steps: photo-induced charge generation, migration, and surface utilization. Efficient light absorption constitutes the fundamental prerequisite. At present, thermodynamic regulation of charge separation *via* structural engineering is conducted. Furthermore, the kinetics of surface redox reactions can be optimized by implementing interface catalysis strategies, thereby reducing activation barriers and accelerating interface reactions. Beyond these approaches, interfacial recognition mechanisms enabled by molecular recognition elements and functional groups enhance thermodynamic stability while dynamically refining the electrode–electrolyte interface *via* real-time feedback. The interface regulation engineering is crucial for achieving PEC sensors with exceptional sensitivity, advancing their applicability in precision bioanalysis and environmental monitoring.

3.1 Transfer channel

In the absence of a driving force, the unfavourable electron–hole recombination caused by the random charge flow after the separation of photogenerated carriers largely hinders the photocatalytic activity. The efficiency of the charge diffusion process critically depends on whether the PEC system can provide effective channels for transferring carriers so that they can reach the redox reaction sites.[28–30] The charge transfer channels can be constructed through various strategies, in which the bonding manner and contact area greatly affect the charge transfer channel.[42] In this section, we focus on the recent exploration of charge transfer channel design principles from the following perspectives, including heterojunction conversion and interfacial bonding mode modulation.

3.1.1 Heterojunction conversion. At present, most research focuses on the single semiconductor-modified electrodes, but this method is limited by the wide bandgap of the material itself and the high electron–hole recombination rate, which makes it difficult to meet the sensitivity and detection limit requirements of practical applications. For example, vertically aligned TiO_2 nanotube (TNT) arrays offer advantages such as a larger surface area, enhanced charge transfer, and improved reusability compared to traditional nanoparticle-based photocatalysts. However, the intrinsic wide bandgap of TiO_2 (3.0–3.2 eV) limits its ability to effectively absorb visible light. As a result, the practical use of TiO_2 is still constrained by its high electron–hole recombination rate and low efficiency in utilizing solar energy.[43,44] In response to the above issues, modification methods such as element doping,[45] deposition of precious metal surfaces, and construction of heterojunctions have been proposed to improve sensing performance.[46] Among them, the regulation of heterojunction types can realize precise regulation of space charge layers and band bending, which further establishes efficient charge transfer channels.[44,45]

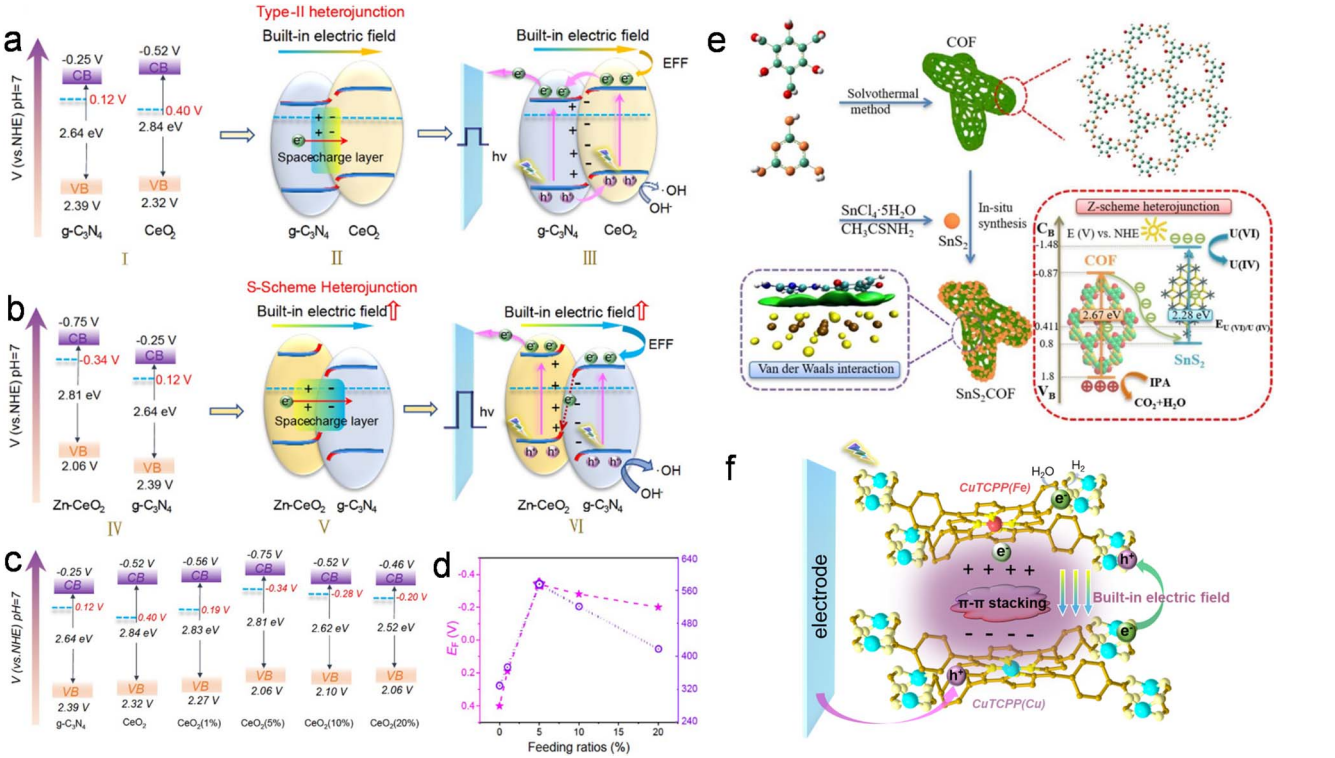

Fig. 3 (a) Schematic diagram of the band structure and charge transfer path of the CeO_2/g-C_3N_4 heterojunction. (b) Schematic diagram of the band structure and charge transfer path of the Zn-CeO_2/g-C_3N_4 heterojunction. (c) Energy-level diagrams of g-C_3N_4, CeO_2 and Zn-CeO_2. (d) Variation of E_F with different feeding ratios.[45] Copyright 2023, Springer Nature. (e) The synthesis route and interaction of SnS_2COF, along with its photocatalytic mechanism for U(VI) reduction.[57] Copyright 2023, Elsevier. (f) Illustrative diagram of the 2D/2D S-scheme heterostructures with strong π−π conjugation and an intense built-in electric field.[62] Copyright 2023, American Chemical Society.

Although type-II heterojunctions can partially enhance the separation efficiency of electron–hole pairs, this charge transfer reduces the redox abilities.[47,48] In contrast, the Z-scheme and S-scheme heterojunctions differ fundamentally in their electron transfer directionality.[49–51] The Z-scheme heterojunction, inspired by natural photosynthesis, employs redox mediators or direct interface charge recombination to stabilize electrons and holes, thereby enhancing photocatalytic activity. The composition of the S-scheme heterojunction can reasonably explain the electron transfer mechanism based on the Z-scheme heterojunction structure, revealing the charge transfer path through the enhancement of a built-in electric field and band bending, which eliminates the requirement for redox media and provides a more direct and efficient charge transfer pathway. It directs charge transfer along optimized pathways, significantly enhancing the redox performance of materials.[52] So far, three experimental approaches can be used to identify S-scheme photocatalysts: (i) *ex situ* and *in situ* irradiated XPS characterization. For oxidation photocatalysts, variations in electron density, observable as shifts in XPS peaks under both illuminated and non-illuminated conditions, provide direct evidence of charge carrier migration across interfaces. (ii) KPFM characterization. KPFM allows for the simultaneous mapping of surface morphology and potential. The surface potential distribution of the material can be readily obtained, revealing the transfer of photo-generated electrons from the oxidizing photocatalyst to the reducing photocatalyst under light irradiation, which is reflected in an increase in the surface potential of the oxidizing photocatalyst. This supports the confirmation of an S-scheme charge transfer pathway. (iii) Electron paramagnetic resonance (EPR) characterization. EPR enables the detection of $^{\bullet}O_2^-$ and $^{\bullet}OH$ radicals, which are indicative of redox processes. The sustained redox ability associated with S-shaped charge transfer can be inferred by analyzing the produced free radicals. Additionally, density functional theory (DFT) calculations can be employed to directly assess the work function and charge densities, providing further insight into interface charge separation and transfer mechanisms.

To improve the interfacial and charge transfer properties of heterojunction-based electrodes, strategies for heterojunction conversion have been developed in recent years. For example, a promising method is introduced based on a novel Zn-doped CeO_2/g-C_3N_4 heterostructure that achieves the transition of charge transfer mechanisms from the original type-II to the advanced S-scheme configuration (Fig. 3a and b). Namely, the conversion of heterojunction types can be achieved by regulating material composition. As a result, a Zn-dependent volcano-type correlation was systematically established to precisely regulate the E_F of CeO_2 through atomic doping strategies. In combination with the conduction band and E_F, the band structures are shown in Fig. 3c. Zn-CeO_2(5%)/g-C_3N_4 with optimized E_F had the best PEC response (Fig. 3d), thereby

significantly improving photoelectric conversion efficiency, implying that the heterojunction conversion can achieve the separation of photogenerated charges.[45] This conversion breaks through the bottleneck of weakened redox ability in type II heterojunctions and significantly improves charge separation efficiency through atomic-level charge channels and electric-field-driven transport.

3.1.2 Interfacial bonding mode modulation. In addition to heterojunction conversion through adjustment of E_F, interface bridging can also be formed through interface bonding mode modulation to reduce interfacial energy barriers and enable rapid charge transfer.[53] Typically, the interfacial interactions of heterojunction photocatalysts can be classified into three types: (i) physically adsorbed interfaces;[54] (ii) intermolecular π–π interaction interfaces for van der Waals heterojunction photocatalysts;[55] (iii) chemically bridged interfaces in heterojunctions.[56]

Among them, the van der Waals force interaction shows more flexibility and convenience. Liu *et al.* constructed an organic–inorganic heterojunction material (SnS_2COF) by the combination of a COF and layered semiconductor SnS_2 through van der Waals force (Fig. 3e).[57] In addition, the large contact area of van der Waals interactions promotes the rapid migration of photo-generated charge carriers. Meanwhile, the separation of photo-generated electrons and holes is promoted in the presence of an internal electric field. Generally, from the viewpoint of intimate contact, the utilization of ultra-thin, sheet-like nanostructures to construct 2D/2D heterojunctions offers the advantage of an expanded interface contact area, thereby reducing the carrier transport distance.[58–60] However, the presence of lattice mismatches between distinct components can introduce substantial resistance at the heterojunction interface, impeding efficient carrier transfer. Consequently, in two-dimensional heterojunctions dominated by van der Waals forces, increasing the interface contact area to establish effective charge transfer pathways has become a promising strategy to alleviate this limitation. Compared with electrostatic adsorption, enhancing intermolecular interactions through π–π conjugation is widely regarded as a method for regulating the interfacial properties of organic semiconductors.[61] Zhu *et al.* proposed an S-scheme heterojunction based on a 2D/2D dual-metalloporphyrin metal organic framework, CuTCPP(Cu)/CuTCPP(Fe), by modulating the central metal atoms (Fig. 3f). The resulting heterojunction exhibited a large built-in electric field, offering a substantial driving force for efficient charge carrier separation and migration. The ultra-thin nanosheet structure reduces the distance of carrier migration by enhancing the interface contact area, while the similar porphyrin main chain promotes reasonable interface matching, thereby suppressing the recombination of photo-generated carriers.[62]

Interface bonding mode modulation can control bulk charge separation and transfer by enhancing the internal polarity electric field. This can be achieved through atomic doping to change the interface bonding type. For example, Ni-doped $Zn_{0.2}Cd_{0.8}S$ quantum dots, which were screened through DFT simulation, were coupled with TiO_2 microspheres to form an S-scheme charge transfer system (Fig. 4a). To enhance H_2 adsorption, DFT calculations are initially carried out to identify the optimal dopant for modifying $Zn_{0.2}Cd_{0.8}S$. The increased built-in electric field in the S-scheme heterojunction results from strengthened interfacial interactions through Ni–O

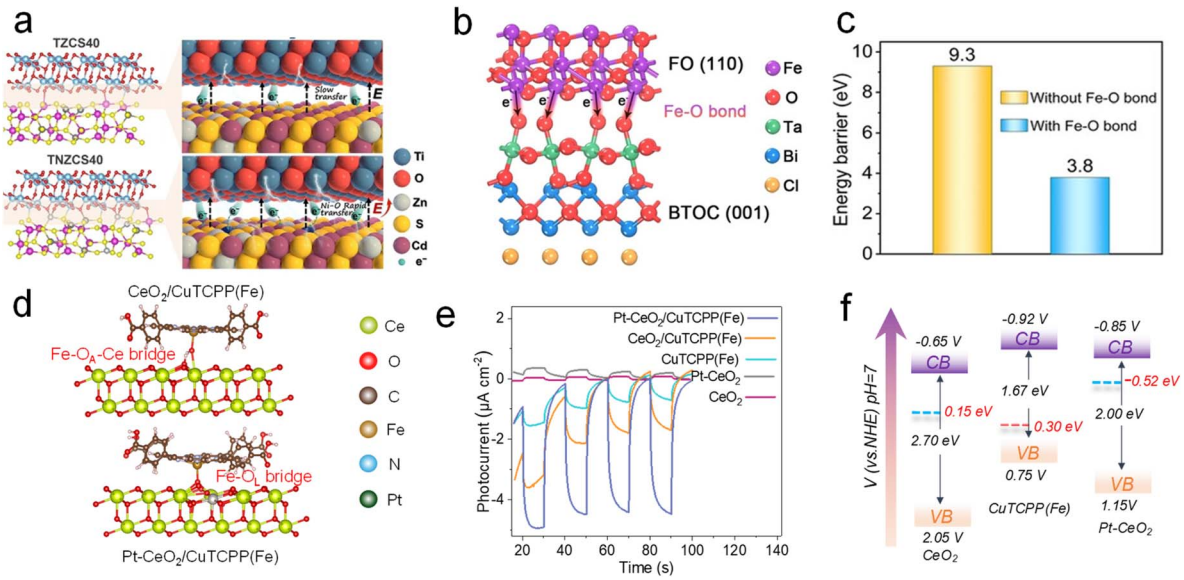

Fig. 4 (a) Schematic depiction of electron transfer of TZCS40 and TNZCS40 driven by internal electric fields (*E*).[38] Copyright 2023, John Wiley and Sons. (b) Schematic depiction of the interfacial Fe–O bond between the FO(110) facet and BTOC(001) facet. (c) Comparison of interfacial charge transfer energy barriers without and with Fe–O bond formation.[39] Copyright 2022, John Wiley and Sons. (d) Diagrammatic illustration of interface chemical bond optimization *via* atomic-level Pt doping to boost PEC efficiency. (e) Photocurrent response. (f) Schematic depiction of the energy bands of CeO_2, Pt-CeO_2 and CuTCPP(Fe).[40] Copyright 2025, Oxford University Press.

bonding and a reduced energy barrier.[63] In contrast to electrostatic interactions, which are prone to electron–hole recombination, chemical bonds provide a more effective means of promoting charge migration due to their stronger atomic interactions compared to hydrogen bonds, electrostatic forces, and van der Waals interactions.

Specifically, the chemically bridged interface serves as an effective charge transfer channel for efficient carrier separation. Chemical bonds can maintain strong redox and light-harvesting capabilities in light energy conversion and storage applications. They influence the interfacial electronic structure, accelerate charge transfer, and achieve the separation of photogenerated carriers.[64,65] Therefore, it is crucial to design high-quality interfaces in heterostructures in a reasonable manner to guide interface charge transfer. Recently, Huang *et al.* developed innovative dot-on-plate Z-scheme heterojunctions by *in situ* anchoring α-Fe_2O_3 nanodots onto the surface of Bi_4MO_8Cl (M = Nb, Ta) nanoplates, creating interfacial chemical bonds and an internal electric field. For simplicity, α-Fe_2O_3 and Bi_4TaO_8Cl are referred to as FO and BTOC, respectively. The interfacial interaction and electron flow direction between FO(110) and BTOC(001) are mediated by the Fe–O bond (Fig. 4b). When FO and BTOC interact through van der Waals forces, electron transfer from BTOC to FO faces a significant energy barrier of 9.3 eV. Nevertheless, the energy barrier can be reduced to 3.8 eV through an interfacial Fe–O chemical bond (Fig. 4c), indicating that electron transfer along the Fe–O bond is more advantageous in terms of energy and space.[66]

Constructing chemical bonds at heterojunction interfaces provides a promising approach to enhance the interfacial transfer of photogenerated charge carriers. However, deliberate modulation of these interfacial chemical bonds is difficult to achieve. Zhu *et al.* presented the synthesis of a p–n junction formed by atomic-level Pt-doped CeO_2 and 2D metalloporphyrin metal–organic framework nanosheets, Pt-CeO_2/CuTCPP(Fe). The introduction of Pt doping at the atomic scale into CeO_2 enhances the density of oxygen vacancies and induces lattice oxygen distortion, which in turn reduces the adsorbed oxygen. This facilitates a shift in the coordination of Fe with oxygen from indirect axial bonds (Fe–O_A) to direct axial bonds with lattice oxygen (Fe–O_L). This transition alters the charge flow at the interface, directing it from Fe–O_A–Ce to Fe–O_L, thereby shortening the carrier transport pathway along the atomic-level charge transport route (Fig. 4d). As a result, this modification leads to a 2.5-fold enhancement in PEC performance compared with CeO_2/CuTCPP(Fe) (Fig. 4e). Furthermore, these chemical bonds lower the interfacial energy barrier and reduce the carrier transport distance, thereby improving charge transfer efficiency. This interaction facilitates the formation of unique heterostructure interfaces, in which chemical bonds mediate interfacial interactions. These chemical bonds act as specific "bridges" that enhance charge transfer between semiconductors, contributing to the overall efficiency of the system.[60,67] In general, the E_F difference determines the strength of the built-in electric field. Pt atom doping increases the discrepancy in E_F between semiconductors, thus enhancing the built-in electric field for fast charge transfer (Fig. 4f). Adjusting semiconductor lattice atoms and optimizing interface bonding modes will provide more opportunities for establishing effective interface chemical bonds and gaining a deeper understanding of transition mechanisms. Furthermore, the establishment of chemical bonding at interfaces can function as a pathway for electron transfer at the atomic scale. These strategies enable efficient signal transduction, which is critical for high-performance sensing applications.

3.2 Interface catalysis

Current strategies in PEC sensing systems predominantly focus on enhancing light-harvesting efficiency and optimizing charge transfer dynamics. However, the often-overlooked challenge lies in the sluggish redox reactions at the photoelectrode/electrolyte interface. This oversight can result in significant photocorrosion of the semiconductor, driven by the accumulation of surface photogenerated charge carriers. Consequently, introducing efficient cocatalysts to promote interfacial redox reactions can further construct high-performance PEC biosensors.[68–71] One promising approach to address this issue involves interfacial catalysis, which mitigates charge recombination by optimizing the interfacial band energetics and catalytic kinetics, thereby enhancing operational stability.

3.2.1 Cocatalyst loading. Cocatalysts are frequently employed as reaction sites to facilitate surface reactions. Given that photogenerated charges can be rapidly consumed on cocatalysts, these materials play a dual role in photocatalysis: one is to reduce the overpotential required to drive the catalytic process, while also enhancing charge separation and transport through the formation of junctions or interfaces.[38,68,72] In this section, we will try to illustrate the intrinsic roles and mechanisms of cocatalysts. Additionally, the catalytic processes involving photogenerated charge separation and transfer will also be included.

Recent studies have highlighted that the incorporation of individual atoms into photoactive materials can serve as active sites, thereby accelerating interfacial reaction kinetics while improving charge separation efficiency. Single-atom catalysts (SACs), which consist of isolated metal atoms dispersed on suitable supports, have been extensively investigated across various domains, including electrocatalysis,[73] photocatalysis,[74] and biomimetic catalysis,[75] owing to their high catalytic activity, special electronic configuration, and clear active sites.

To enhance the photoelectric conversion mechanism, accelerate the directional migration of charge carriers, and improve interfacial reaction kinetics, effective control of the solid–liquid interface is essential. Zhu *et al.* demonstrated that well-defined Fe single-atom catalysts (Fe SACs) were effectively integrated onto the surface of semiconductors (Fig. 5a), thereby enhancing PEC signals through the promotion of the oxygen reduction reaction (ORR). Fe SACs featuring atomically dispersed FeN_4 active sites have been widely recognized for their superior performance in the ORR compared to N–C.[76] As shown in Fig. 5b, the ORR activity of Fe SACs is assessed using cyclic voltammetry (CV) in 0.1 M PBS solution (pH = 7.4) under both N_2 and O_2 saturation. In N_2-saturated electrolyte, where

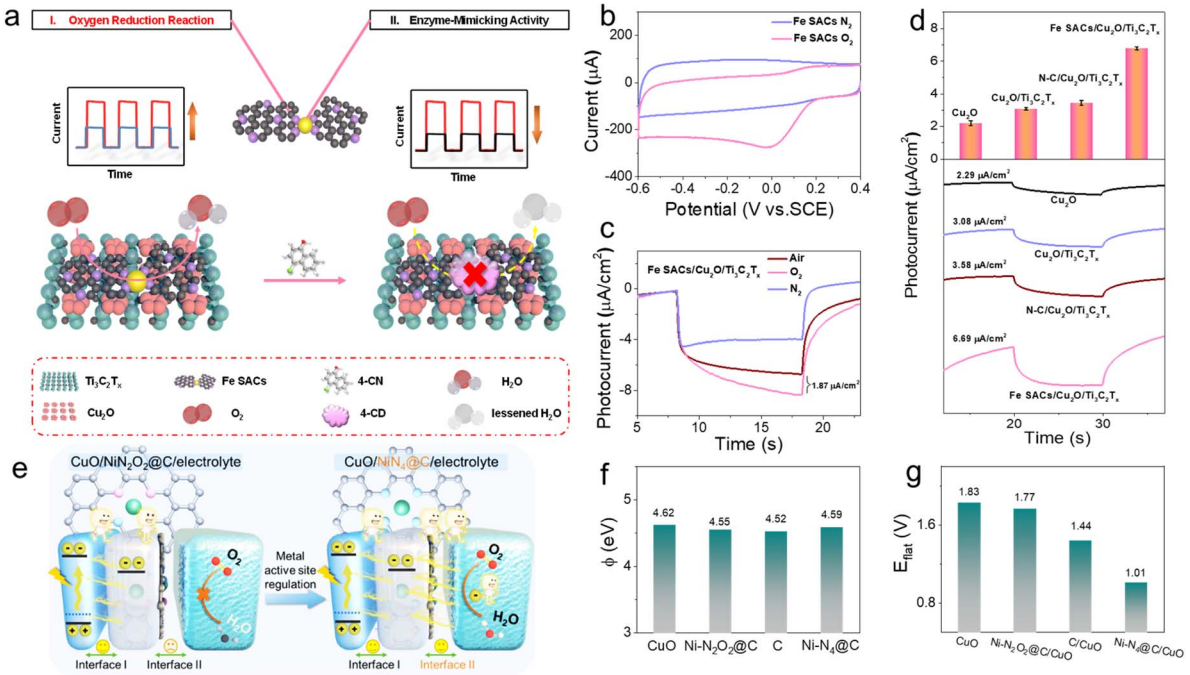

Fig. 5 (a) Schematic view of the operation of the Fe SACs/Cu_2O/$Ti_3C_2T_x$ PEC analytical system, with the expected photocurrent modulation resulting from bifunctional Fe SACs. (b) CV curves of Fe SACs recorded in 0.1 M PBS (pH 7.4) under N_2 and O_2. (c) Photocurrent responses of Fe SACs/Cu_2O/$Ti_3C_2T_x$ in the air, O_2, and N_2 saturated-buffer electrolyte, respectively. (d) Photocurrent responses for Cu_2O, Cu_2O/$Ti_3C_2T_x$, Fe SACs/Cu_2O/$Ti_3C_2T_x$, and N–C/Cu_2O/$Ti_3C_2T_x$.[32] Copyright 2022, American Chemical Society. (e) Illustrative diagram of the PEC process based on tuning metal active sites in the photocathode electron transport layer. (f) Work function comparison of CuO, Ni–N_2O_2@C, C, and Ni–N_4@C. (g) Flat band potential comparison of CuO, Ni–N_2O_2@C/CuO, C/CuO, and Ni–N_4@C/CuO.[77] Copyright 2023, the Royal Society of Chemistry.

dissolved O_2 is purged, a minimal photocurrent is detected for the Fe SACs/Cu_2O/$Ti_3C_2T_x$-based photoelectrode (Fig. 5c). Subsequently, photocurrent responses of different samples were measured under on–off light irradiation (Fig. 5d). As anticipated, the Fe SACs/Cu_2O/$Ti_3C_2T_x$-modified photoelectrode exhibits a notable PEC signal, approximately 2.2 times higher than that of Cu_2O/$Ti_3C_2T_x$. The enhancement in PEC performance can be attributed to the accelerated interfacial ORR process, which reduces charge carrier accumulation and minimizes interfacial charge recombination.

Notably, the strong interaction between the metal atom and the support offers the opportunity to regulate the local environment of the single atom, thereby modulating electron transfer pathways. This regulation can promote the extraction of photogenerated carriers from semiconductor materials and subsequently inject them into the electrolytes, promoting overall device performance.[78] For example, carbon-supported nickel single atoms (Ni SA@C) with catalytic sites of Ni–N_4 and Ni–N_2O_2 were synthesized and integrated with CuO, respectively (Fig. 5e). In terms of the built-in electric field strength formed, due to the similarity of E_F, a similar electron extraction capability is exhibited at the semiconductor/catalyst interface (Fig. 5f). Additionally, the flat band potential (E_{flat}) was measured by the Mott–Schottky (M–S) technique in a 1000 Hz PBS solution (pH = 7.4) (Fig. 5g). As a result, the electrons in the CB of Ni–N_4@C/CuO are more likely to react with O_2, and the driving force is greater due to the high energy level.[77] This approach offers deeper insights into the contribution of cocatalysts, which mainly promote the surface reaction kinetics of photoexcited minority carriers in semiconductor–electrocatalyst photoelectrodes. In addition, the enhanced p-type properties of nickel oxide nanocrystals significantly improve their PEC performance in the presence of methanol as a sacrificial electron donor. This study demonstrates that nanoscale nickel oxide exhibits superior catalytic and PEC performance compared to its bulk counterpart, primarily due to its higher minority carrier extraction rate. Notably, the incorporation of Pt nanoparticles further enhances the photocatalytic efficiency of NiO. This improvement is attributed not only to Pt reducing reaction overpotential but also to its role in facilitating electron–hole separation at the NiO–Pt interface.[79]

Additionally, the appropriate surface loading of oxygen evolution reaction (OER) cocatalysts plays an important role in terms of promoting charge separation and transport, reducing reaction energy barriers, enhancing oxidation kinetics, and enhancing long-term PEC performance.[72] For example, the incorporation of interfacial oxygen through O_3 treatment enhances the formation of In–O–Sn chemical bonds at the $ZnIn_2S_4$ (ZIS) and SnS_2 (TS) interface, resulting in a $ZnIn_2S_4$–O_3–SnS_2 (denoted as ZIS–O–TS) structure. Additionally, the distinctive morphology of ZIS–O–TS serves as an effective cocatalyst, facilitating the transfer of photogenerated holes and mitigating bulk recombination. Experimental results, supported by theoretical simulations, reveal that the In–O–Sn bond

accelerates carrier transport between the interface and bulk, increases the density of active sites, and lowers the surface overpotential for the OER.

Through the dual effects of interface chemical bond band regulation and cocatalysts, a significant increase in photocurrent was achieved while reducing OER overpotential, providing a new strategy for efficient PEC performance. The introduction of OER cocatalysts can notably improve the stability of traditional photoanodes by increasing charge extraction efficiency and minimizing surface self-oxidation. However, modifying only a single cocatalyst is inadequate to fully overcome the issues of low catalytic efficiency and stability commonly seen in conventional photoanodes. This limitation arises from the amorphous or porous characteristics of the catalyst film, which leave certain regions of the semiconductor exposed to the electrolyte despite the deposition of the cocatalyst. Consequently, more advanced and precise interface engineering is required to achieve interface strategies for high-performance PEC system.

3.2.2 Charge extraction layer. Specifically, photoelectrodes incorporating semiconductors and cocatalysts have attracted considerable attention due to their ability to reduce photogenerated charge carrier recombination, promote charge separation and transfer, and enhance surface reaction kinetics. However, the energy level mismatch between the semiconductor and cocatalyst remains a significant challenge, hindering the efficient extraction of photogenerated carriers to the active sites of the cocatalyst. This mismatch leads to substantial recombination at the semiconductor/cocatalyst interface, diminishing the thermodynamic driving force for the interface reaction. To address this, the integration of an electron extraction layer facilitates direct electron transfer, reducing recombination, enhancing charge separation efficiency, and improving the interface quality. This section further explores interface catalysis through potential electronic interactions between the charge extraction layer and the cocatalyst, which influence the kinetics of interface reactions. The electron extraction layer must align with the energy levels of both the semiconductor and cocatalyst to ensure efficient electron transfer from the semiconductor to the cocatalyst. The interaction of electronic states between these components is crucial to ensure that electrons flow through the interface unimpeded.

A novel strategy for electron extraction layers has been introduced, combining platinum nanoclusters and iron single-atom catalysts (Pt_{NC}/Fe–N–C) with a semiconductor to resolve the interface mismatch issue (Fig. 6a). Upon contact, an ohmic contact forms between CuO and platinum nanoclusters (Pt_{NC}), promoting efficient carrier extraction from the semiconductor. The solid–liquid interfacial charge transfer rate for CuO@Pt_{NC}/Fe–N–C ($K_{eff} = 3.65$) is found to be 4.6 and 3.1 times greater than that for CuO ($K_{eff} = 0.79$) and CuO@Fe–N–C ($K_{eff} = 1.17$), respectively (Fig. 6b and c), which highlights the pivotal role of Pt_{NC} in modulating the Fe–N–C interface to enhance the kinetics of solid–liquid interfacial reactions.[80] Furthermore, the Fe SACs on the carbon supports act as stable anchors for Pt_{NC}, creating strong interactions that establish a distinctive Pt–Fe charge transfer pathway, which enhances the interfacial ORR kinetics.

In addition, the severe electron–hole recombination at the $BiVO_4$/oxygen evolution cocatalyst (OEC) interface still limits the PEC performance. Developing an efficient electron–hole separation pathway between $BiVO_4$ and OECs is essential for enhancing PEC performance. One promising approach to achieve this is the use of a hole extraction layer (HEL). Rapid extraction of holes can effectively minimize charge recombination and improve the modest thermodynamic driving force for water oxidation. A thin film of cadmium sulfide nanosheets (CdS NSs) is deposited onto the $BiVO_4$ surface (Fig. 6d), followed by the construction of a series of hole transport molecules (HTs) with tunable energy band structures on the $BiVO_4$|CdS composite. These HT molecules are uniformly anchored on the CdS NSs and form a monolayer *via* disulfide bonds. Under suitable thermodynamic conditions, photogenerated holes are efficiently extracted by the HTs (Fig. 6e). The oxidized HT molecules (HT^+) then undergo isoenergetic hopping between adjacent HT molecules, ultimately transferring oxidative equivalents to the OEC. The outer surface is then coated with a thin layer of an OEC (CoBi). This heterostructure, with its cascading energy band alignment, strongly drives photogenerated holes from $BiVO_4$ to the CoBi surface, enhancing PEC performance. Notably, the $BiVO_4$ (BVO)|CdS-triphenylamine (TPA)|CoBi configuration exhibited the highest charge transfer efficiency across a wide range of applied potentials, demonstrating excellent charge separation capability (Fig. 6f). The strategy of interface catalysis to accelerate reaction dynamics and enhance durability has become a significant method for improving the charge transport efficiency in PEC sensing. This interface engineering strategy advances cocatalyst design for enhanced energy conversion and sensing applications by simultaneously addressing carrier dynamics and interfacial reaction barriers.

3.3 Interface recognition

Chemical recognition of target analytes, coupled with optically modulated electrochemical readouts, enables the precise detection of a wide range of analytes. By strategically designing small-molecule recognition units, dynamically modulating interface structures, and optimizing biocompatibility, interface recognition strategies have emerged as crucial elements in improving the performance of PEC sensors. The integration of these strategies in PEC sensing has led to significant advancements in detection sensitivity, selectivity, and resistance to interference. Furthermore, innovative interfacial recognition elements have been explored to enhance exciton energy transfer efficiency, presenting an alternative to traditional biomolecular recognition probes. This advancement could substantially propel the development of PEC bioassays.

3.3.1 Small molecule probes. A novel *in situ* sensitization approach using small-molecule probes enables the development of efficient PEC biosensors, replacing traditional biomolecular recognition elements. *In situ* sensitization refers to a real-time and dynamic interface functionalization strategy in

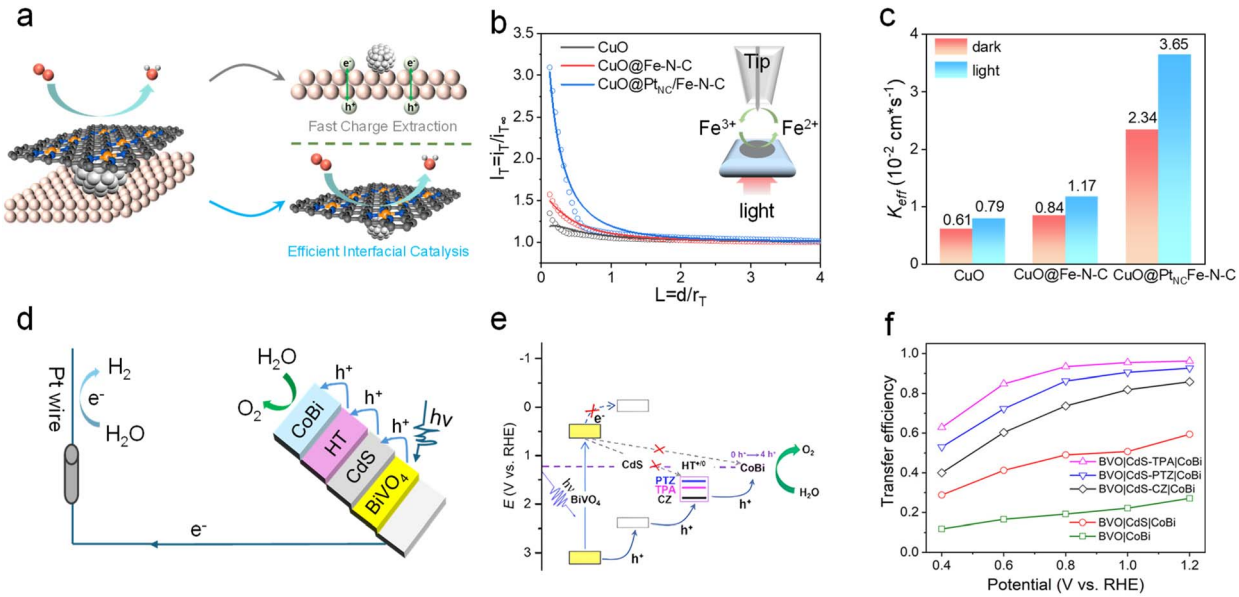

Fig. 6 (a) Design principles of photoelectrodes for strategies involving dual interface modulation. (b) SECM feedback mode approach curves normalized for a Pt ultramicroelectrode (UME) approaching various samples. (c) The rate constant (K_{eff}) of the samples was determined under light and dark conditions.[80] Copyright 2025, Springer Nature. (d) Preparation of the BVO|CdS-HT|CoBi photoanode. (e) The process of photogenerated carrier transfer. (f) Charge transfer efficiency obtained from IMPS spectra of different photoanodes at various potentials.[81] Copyright 2022, American Chemical Society.

PEC sensing. Its core is to trigger the generation or signal amplification mechanism of photoactive materials directly on the electrode surface through the specific binding of small molecule probes to target substances. For example, small molecule silane probes are modified on the surface of graphitic carbon nitride to form a stable interfacial layer (SP-C_3N_4) through chemical bonding (Fig. 7a). This design not only avoids the inhibition of photoelectric signals by the insulation of traditional biomolecules such as antibodies, but also generates Si nanoparticles (SN-C_3N_4) *in situ* through a specific reaction between silane and the enzyme-catalyzed hydrolysis product hydroquinone, constructing a Si/g-C_3N_4 heterojunction interface. This facilitates electron transfer from Si NPs to g-C_3N_4 with O–Si bonds as energy transfer channels, leading to a strong built-in electric field.[82]

Photocurrent regulation in PEC systems is achieved through fluorescence resonance energy transfer (FRET), where the emission of the energy donor is modulated by the target SO_2 concentration, influencing the photocurrent of the photoactive material.[83] This light-modulation approach circumvents selectivity issues, while the fabricated PEC microelectrodes demonstrate commendable stability and reproducibility *in vivo*. A coumarin dye, cSO_2, selectively binds SO_2, serving as both the recognition unit and energy acceptor. FRET between upconversion nanoparticles (UCNPs) and cSO_2 is governed by SO_2 levels, while UCNP luminescence modulates the photocurrent of CdTe quantum dots combined with multiwalled carbon nanotubes (CdTe/MWNTs). This FRET-modulated PEC sensor exhibits high selectivity for SO_2. In *ex vivo* studies, sulfite, representing SO_2 in equilibrium with bisulfites and sulfites in biological systems, was used to probe the PEC microelectrode's photocurrent response, which correlates with sulfite concentration, enabling quantitative detection. Since SO_2 equilibrates with aqueous bisulfites and sulfites (1 : 3, m/m) in biosystems, sulfite was used to represent SO_2 in *ex vivo* investigations. The photocurrent signal of the PEC microelectrode was dependent on the concentration of sulfite, providing an opportunity to quantitatively detect the target. Besides, this FRET-based PEC coupling signal amplification strategy achieves a detection limit as low as 46.5 nM. Moreover, this approach can be generalized to detect other small molecules (*e.g.*, NO and H_2S) by replacing the dye recognition units with aptamers or metal–organic frameworks, offering a versatile platform for the *in vivo* monitoring of electrochemically inactive species. Additionally, by establishing the quantitative structure–activity relationship model of "crystal configuration molecular recognition carrier transport", the three-dimensional layered TiO_2 nanoflower (3D HTNF) photoelectrode with the {110} plane as the main surface has been developed.[84] An integrated PEC biosensor was further developed by combining a microelectromechanical system (MEMS) signal acquisition module. It has been demonstrated through experimental means that the specific recognition of uric acid (UA) molecules on the crystal surface can trigger a significantly positive photocurrent response, which elucidates the interplay mechanism of the crystal surface tuning energy band structure and the interfacial kinetics of response.[85,86]

3.3.2 Docking mode recognition. Traditional biosensors rely on biological recognition units, such as antibodies and aptamers, which suffer from fragility, irreversible binding, poor selectivity, and susceptibility to degradation *in vivo*, limiting the performance of implantable sensors.[67–69] Recently, Zhang *et al.* developed photoelectrodes that utilize atomic anchoring

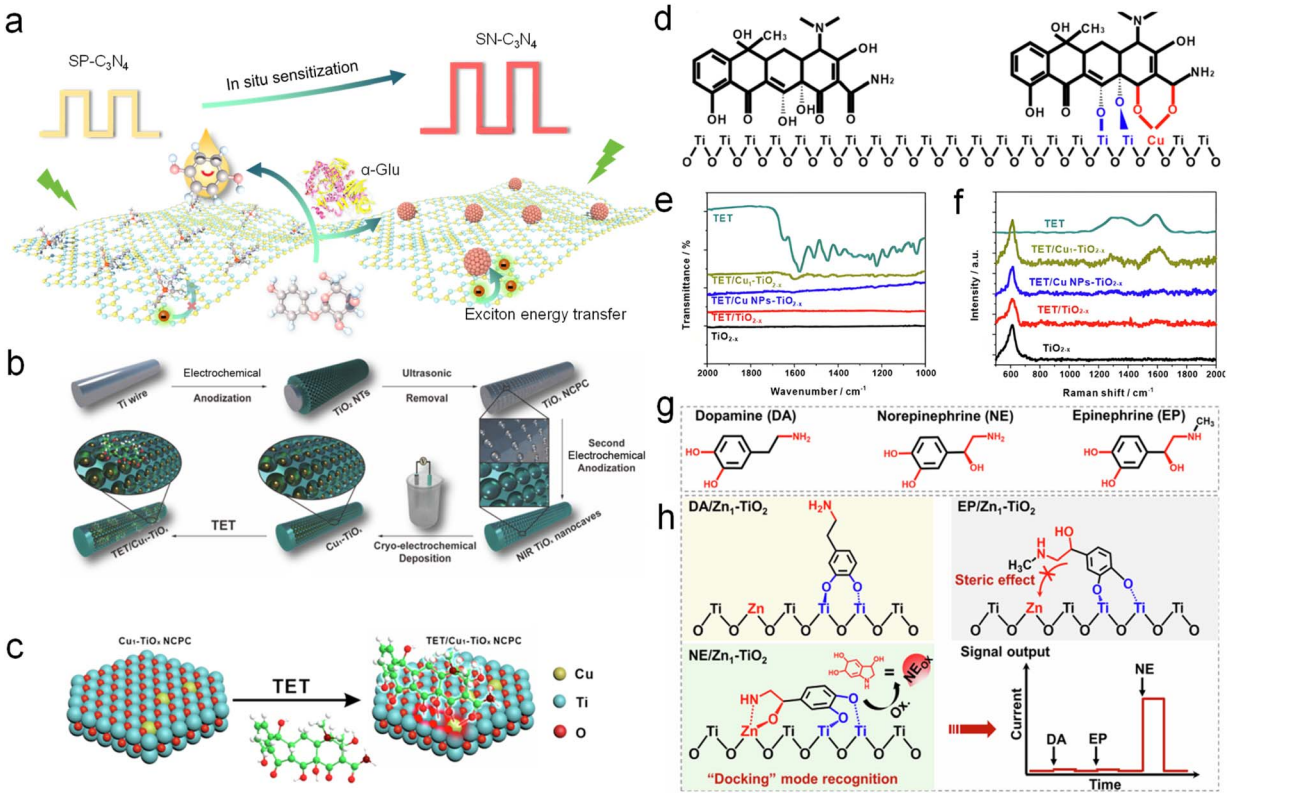

Fig. 7 (a) Schematic illustration of the *in situ* sensitized PEC biosensor using a silane probe.[82] Copyright 2023, American Chemical Society. (b) Schematic illustration of the synthesis processes of Cu_1–TiO_{2-x}. (c) Schematic illustration of the triple-site recognition unit of Cu_1–TiO_{2-x} for TET capture. (d) Coordination of a dual-carbonyl group with Cu_1 and an adjacent dual-hydroxyl group with Ti sites. (e) FTIR spectra and (f) Raman spectra of TiO_{2-x}, TET/TiO_{2-x}, TET/Cu NPs–TiO_{2-x}, TET/Cu_1–TiO_{2-x}, and TET.[27] Copyright 2024, Springer Nature. (g) Chemical structure formula of NE, DA, and EP. (h) Schematic mechanism of NE, DA and EP binding on the Zn_1–TiO_2 photoelectrode and selective photocurrent response of NE with the chemical structure of NE_{OX} representing the final NE reaction product.[87] Copyright 2025, Springer Nature.

technology for the precise immobilization of antibiotic molecules, enhancing target molecule recognition. The atomic dispersion of Cu atoms on a TiO_{2-x} substrate (Cu_1–TiO_{2-x}) provides a promising approach to creating synergistic anchoring sites, thereby facilitating the efficient and selective capture of tetracycline (TET) molecules (Fig. 7b). The recognition mechanism of tetracycline (TET) on Cu_1–TiO_{2-x} is shown in Fig. 7c, where Cu single atoms on the TiO_{2-x} surface coordinate with the dual-carbonyl group of TET (red, Fig. 7d), and adjacent Ti sites bond with its dual-hydroxyl group (blue, Fig. 7d). This triple-site recognition unit selectively captures molecules with a matching structure, significantly improving selectivity and avoiding false positives. The strong interaction between recognition unit elements on the electrode surface eliminates the need for biological components, ensuring stability and robustness for *in vivo* applications. FTIR and Raman spectra confirmed selective TET adsorption on Cu_1–TiO_{2-x}, validating the triple-site recognition strategy (Fig. 7e and f). By exploiting these molecular interactions, implantable PEC sensors with Cu_1–TiO_{2-x} photoelectrodes, encapsulated in an antifouling layer formed *via in situ* metal–organic framework synthesis, enable the selective capture and identification of TET molecules, allowing long-term *in vivo* monitoring of TET metabolism.[27]

Similarly, a Zn single-atom (Zn_1–TiO_2) PEC biosensor integrated onto a TiO_2 substrate has been developed for selective *in vivo* detection of norepinephrine (NE). The biosensor employs a cooperative three-point molecular recognition mechanism for NE binding to Zn_1–TiO_2 (Fig. 7g). Specifically, the *o*-phenol hydroxyl group of NE coordinates with two Ti ligands, and the hydroxyl and primary amine groups form a stable five-membered ring with Zn single atoms, facilitating a "lock-in" binding mode at the cooperative atomic anchor sites (Fig. 7h). This interaction enhances NE adsorption, while photogenerated holes oxidize NE to NE_{OX}, which detaches from the Zn_1–TiO_2 surface. In contrast, dopamine (DA) and epinephrine (EP) are unable to bind due to the steric hindrance and lack of dual recognition sites.[87] Thus, the Zn_1–TiO_2 photoelectrode enables the precise detection of NE, distinguishing it from DA and EP. The Zn_1–TiO_2 electrode shows significantly greater photocurrent variation in response to NE, even at 50-fold higher concentrations of DA and EP, confirming its selective detection capability. Additionally, the biosensor distinguishes NE from serotonin (5-HT) and its metabolites (DOPET and DOPEGAL) and other potential interferents, including artificial cerebrospinal fluid (aCSF). These findings underscore the promising potential of Zn_1–TiO_2 for selective recognition of NE, showing superior anti-interference ability even in the presence of

Table 1 The advantages and disadvantages of the three types of interface engineering

Type	Samples	Advantages	Disadvantages
Charge transfer channel	Zn-CeO_2/g-C_3N_4 (ref. 45)	Realizing the conversion of heterojunction types	Continuous control of delicate Fermi levels is required
	Pt-CeO_2/CuTCPP(Fe) (ref. 40)	Regulating chemical bonds to reduce the carrier transport distance	Tuning the lattice atoms of the semiconductor is required
	CuTCPP(Cu)/CuTCPP(Fe) (ref. 62)	Enhancing interfacial interaction and shortening the carrier transport distance	Materials with a large interface contact area are required
Interface catalysis	Fe SACs/Cu_2O/$Ti_3C_2T_x$ (ref. 32)	Investigate the interface catalytic mechanism at the atomic level by accelerating the ORR	The preparation process of SACs is complex
	Ni–N_4@C/Cu (ref. 77)	Enhance the reaction driving force and reduce the barriers to photoelectron migration	Atomically dispersed metal sites are required
	CuO@Pt_{NC}/Fe–N–C (ref. 80)	Achieve rapid carrier extraction and improve interfacial reaction kinetics	The high cost of noble metal cocatalysts
Interface recognition	SN-C_3N_4 (ref. 82)	Outstanding accuracy and excellent anti-interference ability	Large-scale fabrication of complex heterojunction structures
	CdTe/MWNTs (ref. 83)	Molecular-level specificity and high sensitivity	Specific requirements on the dye molecules
	Zn_1–TiO_2 (ref. 87)	Docking recognition mode exhibits excellent selectivity and stability	Relies on the specific structural features of target molecules

complex *in vivo* environments. The biocompatibility of TiO_2, combined with the stable coordination environment provided by the single zinc atom, ensures the long-term stability and reliability of the sensor for *in vivo* applications. In PEC biosensors, interface recognition is the core hub of signal conversion and amplification. It potentially improves the performance of traditional biosensors by reverse design of customized adsorption sites for specific target molecules and synergistic enhancement of photogenerated carrier separation efficiency. Therefore, interface engineering has become the most critical breakthrough in improving PEC performance by precisely regulating dominant charge separation and interface reaction kinetics. Finally, we have summarized the advantages and disadvantages of the three interface engineering strategies by comparing the representative materials (Table 1).

4 PEC sensors for new pollutant detection

New pollutants are a broad concept that, compared to traditional pollutants, refers to any artificially synthesized or naturally occurring chemicals or microorganisms that exist in the environment and may cause toxic effects and health hazards. We call these compounds new pollutants. Substances such as POPs, antibiotics, microplastics and endocrine disruptors pose considerable environmental risks due to their high toxicity, bioaccumulation potential, and persistent removal challenges. The advancement of interface engineering in PEC sensors has significantly augmented their potential for monitoring emerging pollutants. Through the optimization of electrode material catalytic performance and selectivity, PEC sensors can now sustain high stability and reliability even under complex environmental conditions. Notably, the utility of PEC sensors extends beyond controlled laboratory settings, demonstrating substantial applicability for *in situ* monitoring with remarkable flexibility. Consequently, PEC sensors are poised to drive the future of novel pollutant detection technologies, contributing to global environmental protection efforts and addressing the evolving environmental and public health challenges posed by new pollutants. This strategic focus on diverse environmental targets highlights the adaptability of PEC sensors in addressing various pollutants. Interface engineering exhibits excellent performance in terms of catalytic activity, selectivity, and stability, establishing PEC sensors as essential tools for real-time, on-site monitoring in pollution control and regulatory compliance.

4.1 Persistent organic pollutants

POPs are hazardous to the environment and humans because of their high persistence, bioaccumulation, and toxicity.[88] The widespread use of POPs in daily life has resulted in contamination of ground and surface water worldwide.[89,90] *In vivo* tracking of POPs is crucial for evaluating their ecological and health risks. Existing detection methods are hindered by lethal sampling, complex sample preparation, or bulky equipment. PEC sensing offers high sensitivity with simple instrumentation, providing a more efficient alternative and is a rapidly developing *in vivo* analysis method. A major challenge for *in vivo* PEC sensors is the separation and implantation of multiple electrodes and light sources, leading to issues like biological contamination, electroactive molecule interference, and uncertain electrode placement.

To address this, Li *et al.* developed a coaxial implantable optical fuel microsensor, integrating a fiber-based photoanode

within a glass capillary (GC)-based biocathode. This sensor detects 3,3′,4,4′-tetrachlorobiphenyl (PCB77) with an ultra-low detection limit of 2.8 fg mL^{-1}. The integrated self-powered platform, shown in Fig. 8a, allows *in vivo* tracking of POPs in freely swimming fish brains. As illustrated in Fig. 8b, the photoactive Ag_2S–Bi_2S_3 on the optical fiber (OF) generates electron–hole pairs when excited by red light, while the AA fuel in the GC helps separate the pairs. Due to the band matching between Ag_2S and Bi_2S_3, the excited electrons in Bi_2S_3 transfer to Ag_2S with a relatively negative E_{VB}, then migrate to multiwalled carbon nanotubes (MWNTs) and OF/Au, and finally reach the GC/Au cathode through an external circuit, generating electricity. Addition of PCB77 forms an Apt-PCB77 complex on the cathode, hindering electron–hole pair separation and reducing open-circuit potential (OCP). This sensor can be easily adapted for detecting other pollutants or biomolecules *in vivo*.[91]

Additionally, a 3D layered Cu_2SnS_3@SnS_2 flower with a sandwich Cu_2SnS_3–SnS_2–Cu_2SnS_3 double interface heterojunction assembled from petal-like lamellae was successfully designed and synthesized for PEC sensors, as shown in Fig. 8c. The unique double interface heterostructure combines the 3D flower structure at the same time, which greatly increases light absorption. The composition ratio of Cu_2SnS_3 and SnS_2 is controlled by adjusting the electrodeposition time, so that the Cu_2SnS_3@SnS_2 heterojunction exhibits a dual-mode signal. The Cu_2SnS_3@SnS_2/FTO electrode demonstrates excellent photoelectron reduction for ultra-sensitive detection of trace nitrobenzene (NB) and photoelectron oxidation for selective detection of L-cysteine (L-Cys) without enzymes under light.[92]

4.2 Antibiotics

Quinolones from the 1980s have emerged as vital agents in the treatment of bacterial infections, owing to their broad-spectrum efficacy and established safety profiles. Well-known compounds such as norfloxacin, ciprofloxacin, and ofloxacin have garnered considerable attention in both veterinary and human medicine. However, the extensive use of quinolone antibiotics has resulted in their pervasive presence in environmental systems, raising significant concerns regarding their potential effects on human health and ecosystems. Furthermore, the persistence of these residues contributes to the alarming rise in antibiotic resistance, presenting a toxicological threat to aquatic organisms.[93] Consequently, the trace detection and quantification of these pollutants have become critical for monitoring environmental systems, as well as food and biological samples.

To detect multiple targets, it is very important to develop a bias potential-addressing PEC biosensor. A bias potential-controlled PEC aptasensor for simultaneous detection of enrofloxacin (ENR) and ciprofloxacin (CIP) using $CuInS_2$/3DNG and Bi^{3+}/B-TiO_2/rGO was developed (Fig. 9a). Subsequently, selectivity experiments were conducted on the adapter sensor with other antibiotics, including tetracycline (Tc), tobramycin (TOB), and sulfamethoxazole (SDZ). By showing that these antibiotics compete with ENR and CIP, the change in photocurrent intensity is relatively small, confirming that the sensor exhibits high selectivity for detecting ENR and CIP. Potentiometric photocurrents revealed distinct cathodic and anodic currents for ENR ($CuInS_2$/3DNH) and CIP (Bi^{3+}/B-TiO_2/rGO), respectively. The sensor showed wide linear ranges (ENR: 0.01–

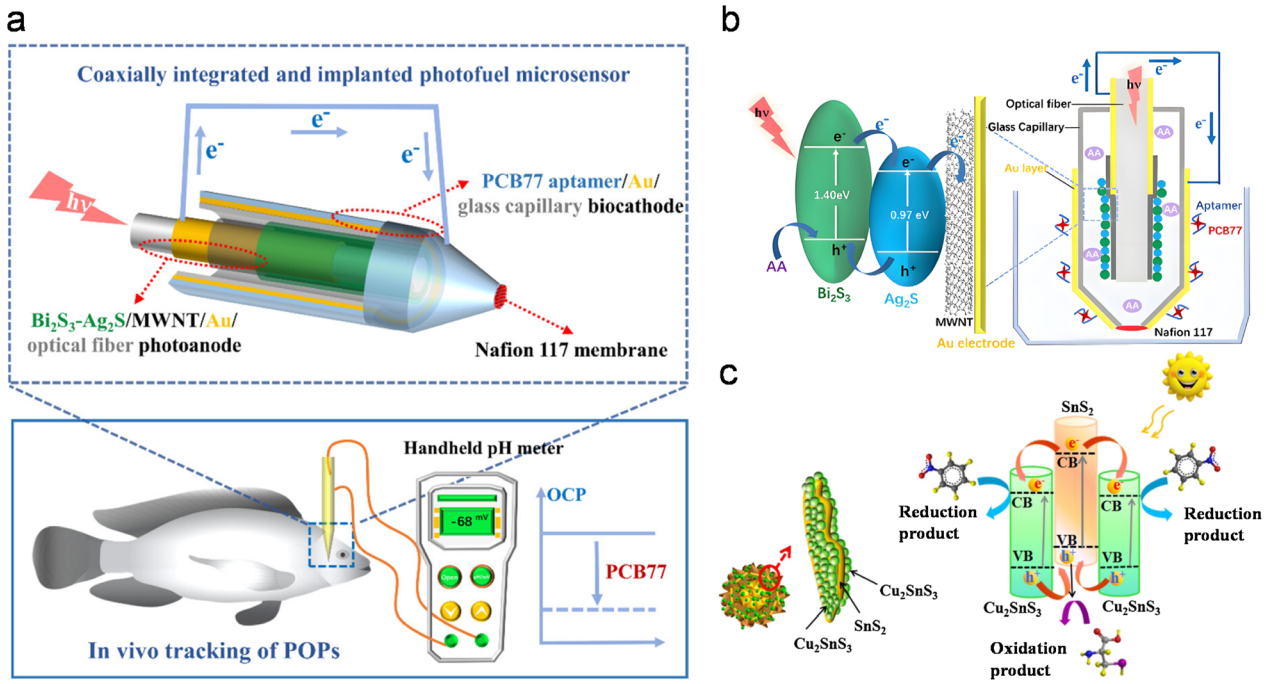

Fig. 8 (a) Schematic diagram of the implanted photofuel microsensor for self-powered *in situ* detection of POPs in a swimming fish brain using a coaxially integrated photoanode biocathode light source platform. (b) Schematic illustration of the developed sensor structure and its sensing mechanism for PCB77.[91] Copyright 2023, American Chemical Society. (c) Schematic of the sensing mechanism and charge transfer in the double p–n heterojunction Cu_2SnS_3@SnS_2 PEC system.[92] Copyright 2019, Elsevier.

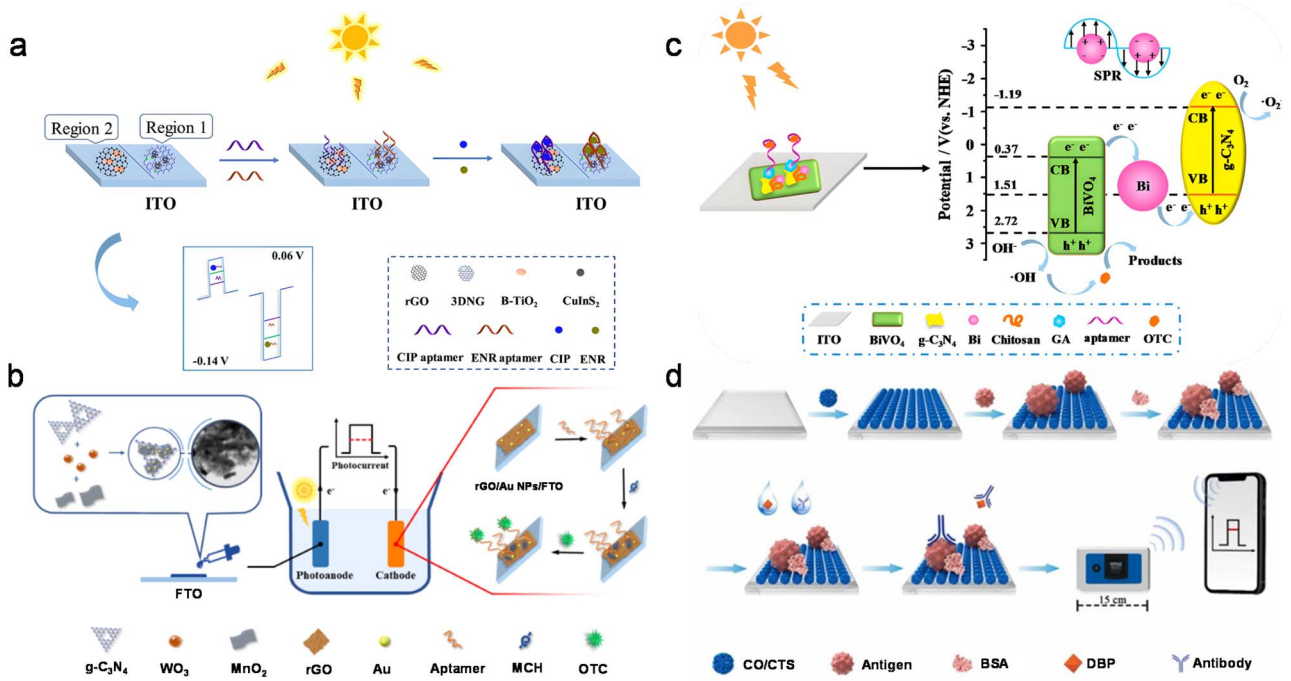

Fig. 9 (a) Fabrication of the PEC aptasensor for detecting two antibiotics.[94] Copyright 2021, Elsevier. (b) Preparation of the sensor platform.[95] Copyright 2021, American Chemical Society. (c) Schematic illustration of the PEC aptasensor for OTC detection based on the Bi/$BiVO_4$/g-C_3N_4 heterojunction.[96] Copyright 2020, Elsevier. (d) Construction process of the PEC POCT platform for detecting DBP.[97] Copyright 2023, Elsevier.

10 000 ng mL^{-1}, CIP: 0.01–1000 ng mL^{-1}) and low detection limits (3.3 pg mL^{-1} for both). Detection in milk samples highlights the potential of sensors for simultaneous antibiotic contaminant monitoring in food.[94]

Recently, a self-powered PEC aptasensor for oxytetracycline (OTC) detection was developed, featuring a dual Z-scheme photoanode and an aptamer-based cathode. The photoanode was constructed by modifying a fluorine-doped tin oxide (FTO) electrode with a ternary WO_3/g-C_3N_4/MnO_2 composite, leveraging the dual Z-scheme heterostructure for enhanced photocurrent generation. A reduced graphene oxide/Au nanoparticle (rGO/Au NP)-modified FTO electrode served as the cathode, replacing traditional noble metal catalysts (*e.g.*, Pt) to reduce cost and eliminate the need for oxygen supply. By combining an aptamer with 6-mercaptohexanol (MCH) for target capture, the cathode achieved both selective recognition of OTC and the formation of a well-aligned DNA monolayer.

This design enabled sensitive, selective, and stable OTC detection by separating light-harvesting and recognition steps.[95] Meanwhile, the Z-scheme heterojunctions, consisting of an electronic mediator and semiconductors with complementary band gaps, not only significantly improved the separation efficiency of photogenerated charge carriers, but also maintained the strong redox ability of electrons and holes. A novel three-component Z-scheme heterojunction, comprising Bi/$BiVO_4$/g-C_3N_4, was synthesized *via* an *in situ* reduction process using $NaBH_4$ as the reducing agent. The plasmonic Bi metal bridges $BiVO_4$ and g-C_3N_4, enabling Z-scheme formation and enhancing electron–hole pair separation (Fig. 9c). The PEC aptasensor demonstrates OTC detection with a wide linear range (0.01–1000 nM) and a low detection limit of 3.3×10^{-3} nM.[96]

4.3 Microplastics

Global concern over micro- and nano-plastics (MNPs) has risen due to their ubiquity and associated risks. Accurate MNP detection is essential for understanding their environmental fate, transformation, and toxicity. Inadequate recycling and uncontrolled emissions have resulted in substantial plastic waste, which may degrade under ultraviolet radiation, mechanical wear and biodegradation, and finally form microplastics (MP, 1 μm to 5 mm). In the contemporary environmental landscape, the pervasive distribution of micro/nanoplastics constitutes a dire threat, necessitating the advent of innovative remediation strategies.

As the main harmful additive released by microplastics and nanoplastics, the identification of dibutyl phthalate (DBP) in complex matrices has attracted increasing attention from environmental monitoring and food safety. Cu_2O/Cu_3SnS_4 nanoflowers used as photoactive materials were first prepared, which can be constructed as a PEC point-of-care test (POCT) based on smartphones (Fig. 9d). The effective energy level matching between Cu_2O and Cu_3SnS_4 accelerates the transfer of photo-generated electron–hole pairs, significantly improving the performance of intelligent PEC POCT. Cu_2O/Cu_3SnS_4 has been proven to be a Z-type heterojunction through DFT calculations. Competitive immunoassay was achieved on the Cu_2O/Cu_3SnS_4 modified electrode, significantly reducing the photocurrent signal and enhancing POCT sensitivity. Smartphones

have been used to record and transmit PEC results. Under optimal conditions, the PEC POCT system demonstrates a linear range of 0.04–400 ng mL^{-1} and a low detection limit of 7.94 pg mL^{-1} in real samples, along with excellent stability, reproducibility, repeatability, and selectivity. It shows strong performance and practicality for DBP detection in water and edible oil samples.[97]

In contrast to the traditional three-electrode system, the self-powered sensor omits the need to combine photoelectric signal conversion and biometrics on the same electrode. The photocathode is dedicated solely to the immuno-recognition process, while the photoanode serves to enhance the photoelectric signal, thereby improving both the stability and sensitivity of the sensor. A self-powered PEC portable sensor (Fig. 10a) combines a photocathode and photoanode for precise, sensitive, and user-friendly detection of polystyrene microplastics (PS MPs). Under optimal conditions, it achieves a detection limit of 0.09 μg mL^{-1} and a linear range of 0.5–1000 μg mL^{-1}. Notably, the sensor exhibits robust resistance to interference from heavy metal ions and organic compounds, maintaining an accuracy exceeding 97% even in the presence of such contaminants.[98]

4.4 Endocrine disruptors

Although endocrine-disrupting chemicals have low concentrations in water, once they enter an organism, they can accumulate and be transmitted from one to another through the food chain, which can lead to cancer or problems with the reproductive and endocrine systems. The self-purification ability of water can alleviate environmental pollution problems to a certain extent, but the continuous accumulation of endocrine-disrupting chemicals will still exceed the self-purification ability of water. Therefore, it is particularly necessary to effectively remove endocrine-disrupting chemicals from water.

The interaction between PEC semiconductor nanomaterial sensitive interfaces and microscopic substances has created infinite potential for effective detection of endocrine disruptors. A highly efficient PEC aptamer sensor, based on Cu_3BiS_3 sensitized CuV_2O_6 nanocomposites, demonstrates excellent visible light PEC performance for the detection of bisphenol A (BPA) (Fig. 10b). By integrating Cu_3BiS_3 nanosheets as photosensitizers, CuV_2O_6 nanowire structures synthesized using a simple hydrothermal method were sensitized. The alignment of the band gaps between Cu_3BiS_3 and CuV_2O_6 facilitates a stable PEC response, leading to an effective interface structure. The surface of the CuV_2O_6/Cu_3BiS_3 electrode is functionalized with a BPA-specific aptamer, which can specifically bind to BPA and accurately quantify its content. The resulting sensor exhibits a broad detection range from 5.00×10^{-1} to 5.00×10^{4} ng mL^{-1}, along with a low detection limit of 1.60×10^{-1} ng mL^{-1} (S/N = 3). Notably, the sensor maintains its stability, repeatability, and reproducibility even after 20 testing cycles and prolonged storage.[99] A novel PEC aptamer sensor for selective BPA detection was developed using ZnO nanopencils activated by Au nanoparticles (Fig. 10c) and surface plasmon resonance (SPR). Light irradiation induces a higher

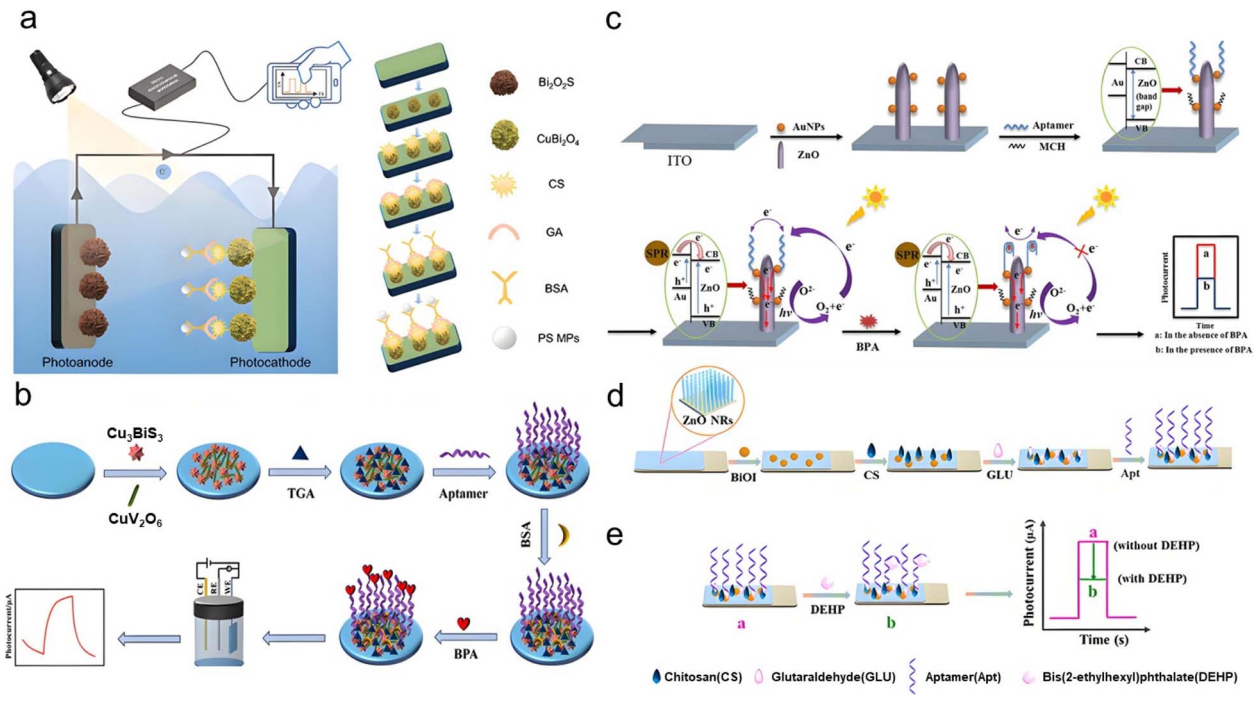

Fig. 10 (a) Schematic diagram of the construction process of a self-powered portable PEC sensor based on a dual-photoelectrode.[98] Copyright 2025, Elsevier. (b) Schematic diagram of the PEC aptasensor construction process.[99] Copyright 2024, Springer Nature. (c) Illustrative diagram of the PEC aptasensor working mechanism for bisphenol A (BPA) using Au-decorated ZnO nanoarrays.[100] Copyright 2016, Elsevier. (d) Illustration of the BiOI/ZnO NR PEC aptasensing platform for DEHP and the construction steps of the platform. (e) The detection recognition mechanism for DEHP.[101] Copyright 2024, Elsevier.

photocurrent in Au/ZnO nanoparticles due to hot electrons from excited gold nanoparticles, compared to pure ZnO. The selectivity of the PEC aptamer sensor for BPA was evaluated by comparing its response to several other common bisphenol compounds, including 4,4′-bisphenol, 6F-bisphenol A, and bisphenol B, all at a concentration of 60 nmol L^{-1}. The interference from these species was minimal, with no more than a 6% impact on BPA determination. This can be attributed to the high specificity of the aptamer for BPA, indicating that the prepared PEC aptamer sensor has superior selectivity. BPA binding induces a conformational change in the aptamer to a G-quadruplex structure, blocking photogenerated electron transport. The sensor successfully detects BPA in drinking water and liquid milk samples.[100]

A PEC biosensor for bis(2-ethylhexyl) phthalate (DEHP) detection was developed using BiOI/ZnO nanoarrays (NRs) as transducers and DEHP aptamers as recognition elements (Fig. 10d and e). ZnO NRs, prepared *via* hydrothermal synthesis, enhance light absorption due to their large surface area. The combination of BiOI and ZnO NRs promotes visible light absorption and charge carrier separation *via* the built-in electric field, yielding a strong photocurrent response. The sensor demonstrates high sensitivity, selectivity, and reproducibility (RSD = 1.6%) for DEHP detection.[101]

5 Conclusion and outlooks

Compared to traditional bulk material modification, interface engineering directly acts on the final utilization of photogenerated carriers, breaking through the bottlenecks of charge separation efficiency, reaction kinetics, and stability through multidimensional structural design and functional integration.[102,103] The semiconductor/electrolyte interface is critical for achieving efficient and stable photoelectrodes and has attracted considerable attention.[104,105] Various interface engineering strategies have been extensively developed, driving rapid advances in the PEC field.

In this review, we first introduced the principles, challenges and advantages of PEC sensing. Then, the interface engineering breaks through the sensitivity and stability bottlenecks of traditional sensing technology by regulating the charge transfer, surface reaction kinetics of photoelectrodes and the novel sensing interface. Finally, the application of PEC sensors based on interface engineering for new pollutant detection was discussed. Moreover, the current interface engineering strategy still has limitations, such as the high cost of noble metal cocatalysts and challenges in large-scale fabrication of complex heterojunction structures. Nevertheless, further insights are required to enhance photoelectrode performance, and real-time, *in situ* monitoring can provide valuable information for this purpose. To design an effective interface for PEC sensing, several factors need to be considered.

5.1 Dynamic interface modulation

Effective real-time tracking and *in situ* measurement can provide important information, such as composition changes and interface changes in the PEC process, which is very important for determining the modification strategy. Using multiple quantitative and visual experiments for collaborative characterization is becoming increasingly necessary. This dynamic modulation not only improves charge carrier separation but also facilitates more efficient charge transfer, thus maximizing the photoelectric response.

5.2 Biomimetic transfer channel engineering

In the natural photosynthesis system, efficient electron flow is achieved through an electron transport chain (ETC), enabling effective directional migration for charge separation. Moreover, the two photosynthetic systems that undergo oxidation and reduction reactions in natural photosynthesis are spatially separated. This emphasizes the potential for collaboration between PEC and biomimetic technology, as demonstrated by the complex photosystem I (PSI) and photosystem II (PSII) systems inherent in photosynthesis. Within this process, the ETC orchestrates the efficient transfer of electrons between PSII and PSI, facilitating effective charge separation. Notably, PSI and PSII engage in distinct oxidation and reduction reactions, occurring in physically separated structural domains, which is crucial for their functional coordination in energy conversion. This inspires us to design artificial photosynthetic systems that simulate natural photosynthesis by combining spatially separated redox sites and directed charge transfer pathways.

5.3 Interfacial catalytic mechanisms

The understanding and optimization of interfacial catalytic mechanisms are paramount to improving the overall efficiency of PEC sensing systems. At the interface between photoactive materials and the electrolyte, catalytic processes govern key reactions, such as charge transfer and redox processes. The investigation of reaction kinetics at interfaces, coupled with the identification of reaction intermediates and the clarification of the roles played by surface interactions and catalytic sites, offers critical insights into the fundamental mechanisms underlying these processes.

5.4 Multiple-target recognition interface

Advancements in PEC sensing also depend on the development of novel strategies for interface recognition. The selective detection of target analytes relies on the design of interfaces that can specifically interact with molecular species of interest. This requires the incorporation of recognition elements, such as functionalized surfaces, molecular imprinting, or tailored receptor molecules, to facilitate selective binding and recognition at the interface. By integrating these strategies, PEC sensors can achieve enhanced specificity, ultrahigh sensitivity, and a wider dynamic range, enabling the simultaneous detection of multiple new pollutants in complex environmental matrices. Such advancements will significantly improve the monitoring of new pollutants, supporting timely risk assessment and regulatory decision-making.

Author contributions

Xiaoyu Dong and Wenhong Yang contributed equally. Xiaoyu Dong: investigation, conceptualisation, writing – original draft, review and editing. Wenhong Yang: conceptualisation, writing – original draft, review and editing. Liuyong Hu: conceptualisation, investigation, writing – original draft, review and editing, and supervision. Wenling Gu: supervision, review and editing, and funding acquisition. Chengzhou Zhu: supervision, writing – original draft, review and editing, and funding acquisition.

Conflicts of interest

There are no conflicts to declare.

Data availability

No primary research results, software or code have been included and no new data were generated or analysed as part of this review.

Acknowledgements

The authors gratefully acknowledge the financial support from the National Natural Science Foundation of China (no. 22474046, 22474103), the Fundamental Research Funds for the Central Universities (no. CCNU24JCPT032), and the Program of Introducing Talents of Discipline to Universities of China (111 Program, B17019).

References

1 W. Tu, Z. Wang and Z. Dai, *TrAC, Trends Anal. Chem.*, 2018, **105**, 470–483.
2 X. Tao, Y. Zhao, S. Wang, C. Li and R. Li, *Chem. Soc. Rev.*, 2022, **51**, 3561–3608.
3 J. Shu and D. Tang, *Chem.–Asian J.*, 2017, **12**, 2780–2789.
4 Y. Gao, J. Tang, Q. Zhou, Z. Yu, D. Wu and D. Tang, *Anal. Chem.*, 2024, **96**, 5014–5021.
5 L. Lu, R. Zeng, Q. Lin, X. Huang and D. Tang, *Anal. Chem.*, 2023, **95**, 16335–16342.
6 W.-W. Zhao, J.-J. Xu and H.-Y. Chen, *Chem. Soc. Rev.*, 2015, **44**, 729–741.
7 W.-W. Zhao, J.-J. Xu and H.-Y. Chen, *Chem. Rev.*, 2014, **114**, 7421–7441.
8 Y. Zang, J. Lei and H. Ju, *Biosens. Bioelectron.*, 2017, **96**, 8–16.
9 J. Lei and H. Ju, *Chem. Soc. Rev.*, 2012, **41**, 2122.
10 A. Chen and S. Chatterjee, *Chem. Soc. Rev.*, 2013, **42**, 5425.
11 A. P. F. Turner, *Chem. Soc. Rev.*, 2013, **42**, 3184.
12 J.-J. Xu, W.-W. Zhao, S. Song, C. Fan and H.-Y. Chen, *Chem. Soc. Rev.*, 2014, **43**, 1601–1611.
13 Y. Li, R. Zeng, W. Wang, J. Xu, H. Gong, L. Li, M. Li and D. Tang, *ACS Sens.*, 2022, **7**, 1593–1601.
14 J. Shu, Z. Qiu, S. Lv, K. Zhang and D. Tang, *Anal. Chem.*, 2018, **90**, 2425–2429.
15 H. Wang, J. Tang, X. Wan, X. Wang, Y. Zeng, X. Liu and D. Tang, *Anal. Chem.*, 2024, **96**, 15503–15510.
16 Y. Gao, Z. Yu, L. Huang, Y. Zeng, X. Liu and D. Tang, *Anal. Chem.*, 2023, **95**, 9130–9137.
17 Y. Qin, J. Wen, L. Zheng, H. Yan, L. Jiao, X. Wang, X. Cai, Y. Wu, G. Chen, L. Chen, L. Hu, W. Gu and C. Zhu, *Nano Lett.*, 2021, **21**, 1879–1887.
18 C. Ding, J. Shi, Z. Wang and C. Li, *ACS Catal.*, 2017, **7**, 675–688.
19 S. Chen, J. Wang, M. Zhou, H. Zhu, Y. Zhang, J. Li, J. Bai, L. Xia, Q. Xu and B. Zhou, *ACS Catal.*, 2020, **10**, 2413–2418.
20 R. Zeng, L. Zhang, Z. Luo and D. Tang, *Anal. Chem.*, 2019, **91**, 7835–7841.
21 J. Li, C.-B. Chen, D.-D. Wang, C.-X. Li, F. Zhang, D.-B. Li, D. Min, W.-W. Li, P. K. S. Lam and H.-Q. Yu, *ACS Sustain. Chem. Eng.*, 2018, **6**, 9591–9595.
22 P. Varadhan, H.-C. Fu, D. Priante, J. R. D. Retamal, C. Zhao, M. Ebaid, T. K. Ng, I. Ajia, S. Mitra, I. S. Roqan, B. S. Ooi and J.-H. He, *Nano Lett.*, 2017, **17**, 1520–1528.
23 Z. Qiu, J. Shu and D. Tang, *Anal. Chem.*, 2018, **90**, 12214–12220.
24 E. Poli, K. H. Jong and A. Hassanali, *Nat. Commun.*, 2020, **11**, 901.
25 L. Liu, J. Hao and K. Wu, *Adv. Funct. Mater.*, 2025, **35**, 2414738.
26 R. Li, Y. Zhang, W. Tu and Z. Dai, *ACS Appl. Mater. Interfaces*, 2017, **9**, 22289–22297.
27 X. Xu, D. Xu, S. Lu, X. Zhou, S. Yang and Z. Zhang, *Nat. Commun.*, 2024, **15**, 8827.
28 Y. Xiang, Y. Kong, W. Feng, X. Ye and Z. Liu, *Chem. Sci.*, 2021, **12**, 12977–12984.
29 G. Chen, Y. Qin, L. Jiao, J. Huang, Y. Wu, L. Hu, W. Gu, D. Xu and C. Zhu, *Anal. Chem.*, 2021, **93**, 6881–6888.
30 Y. Li, D. Liu, S. Meng, N. Dong, C. Liu, Y. Wei and T. You, *Biosens. Bioelectron.*, 2022, **218**, 114759.
31 Z. Hu, H. Wang, H. Chen, G.-C. Fan and X. Luo, *Biosens. Bioelectron.*, 2023, **242**, 115724.
32 Y. Qin, J. Wen, X. Wang, L. Jiao, X. Wei, H. Wang, J. Li, M. Liu, L. Zheng, L. Hu, W. Gu and C. Zhu, *ACS Nano*, 2022, **16**, 2997–3007.
33 X. Wang, X. Rong, Y. Zhang, F. Luo, B. Qiu, J. Wang and Z. Lin, *Anal. Chem.*, 2022, **94**, 3735–3742.
34 R. Tan, Y. Qin, M. Liu, H. Wang, J. Li, Z. Luo, L. Hu, W. Gu and C. Zhu, *ACS Sens.*, 2023, **8**, 263–269.
35 Y. Chen, W. Gu, C. Zhu and L. Hu, *Anal. Chem.*, 2024, **96**, 8855–8867.
36 K. Sivula and R. Van De Krol, *Nat. Rev. Mater.*, 2016, **1**, 15010.
37 T. Yao, X. An, H. Han, J. Q. Chen and C. Li, *Adv. Energy Mater.*, 2018, **8**, 1800210.
38 S. Li, L. Meng, W. Tian and L. Li, *Adv. Energy Mater.*, 2022, **12**, 2200629.
39 X. Tao, Y. Zhao, S. Wang, C. Li and R. Li, *Chem. Soc. Rev.*, 2022, **51**, 3561–3608.
40 P. Wang, Y. Mao, L. Li, Z. Shen, X. Luo, K. Wu, P. An, H. Wang, L. Su, Y. Li and S. Zhan, *Angew. Chem., Int. Ed.*, 2019, **58**, 11329–11334.
41 W.-W. Zhao, J.-J. Xu and H.-Y. Chen, *Biosens. Bioelectron.*, 2017, **92**, 294–304.

42 W. Yang, M. Liu, Y. Qin, R. Xiao, R. Tan, Y. Qiu, W. Jiang, Y. Chen, W. Li, W. Gu, L. Hu and C. Zhu, *Anal. Chem.*, 2025, **97**, 3756–3764.
43 S. Liu, Y. Li, F. Jiang, M. Wang, S. Hou, Y. Li and Q. Wei, *Biosens. Bioelectron.*, 2025, **287**, 117676.
44 J. Zhang, X. Wang, X. Wang and C. Li, *Acc. Chem. Res.*, 2025, **58**, 787–798.
45 M. Liu, J. Wen, Y. Qin, J. Li, Y. Tang, L. Jiao, Y. Wu, Q. Fang, L. Zheng, X. Cui, W. Gu, C. Zhu, L. Hu and S. Guo, *Sci. China: Chem.*, 2023, **66**, 1228–1236.
46 S. Lin, H. Ren, Z. Wu, L. Sun, X.-G. Zhang, Y.-M. Lin, K. H. L. Zhang, C.-J. Lin, Z.-Q. Tian and J.-F. Li, *J. Energy Chem.*, 2021, **59**, 721–729.
47 G. Wang, S. Lv, Y. Shen, W. Li, L. Lin and Z. Li, *J. Materiomics*, 2024, **10**, 315–338.
48 S. Li, W. Xu, L. Meng, W. Tian and L. Li, *Small Sci.*, 2022, **2**, 2100112.
49 F. Xu, K. Meng, B. Cheng, S. Wang, J. Xu and J. Yu, *Nat. Commun.*, 2020, **11**, 4613.
50 B. Zhu, J. Sun, Y. Zhao, L. Zhang and J. Yu, *Adv. Mater.*, 2024, **36**, 2310600.
51 L. Zhang, J. Zhang, H. Yu and J. Yu, *Adv. Mater.*, 2022, **34**, 2107668.
52 Q. Xu, L. Zhang, B. Cheng, J. Fan and J. Yu, *Chem*, 2020, **6**, 1543–1559.
53 Z. Zhao, Z. Wang, J. Zhang, C. Shao, K. Dai, K. Fan and C. Liang, *Adv. Funct. Mater.*, 2023, **33**, 2214470.
54 Y. Li, J. Huang, X. Hu, L. Bi, P. Cai, J. Jia, G. Chai, S. Wei, L. Dai and Z. Wen, *Adv. Funct. Mater.*, 2018, **28**, 1803330.
55 D. Zhao, Y. Wang, C.-L. Dong, Y.-C. Huang, J. Chen, F. Xue, S. Shen and L. Guo, *Nat. Energy*, 2021, **6**, 388–397.
56 X. Wang, X. Wang, J. Huang, S. Li, A. Meng and Z. Li, *Nat. Commun.*, 2021, **12**, 4112.
57 X. Liu, R.-X. Bi, C.-R. Zhang, Q.-X. Luo, R.-P. Liang and J.-D. Qiu, *Chem. Eng. J.*, 2023, **460**, 141756.
58 W. Xu, W. Liu, J. F. Schmidt, W. Zhao, X. Lu, T. Raab, C. Diederichs, W. Gao, D. V. Seletskiy and Q. Xiong, *Nature*, 2017, **541**, 62–67.
59 Z. Xing, J. Hu, M. Ma, H. Lin, Y. An, Z. Liu, Y. Zhang, J. Li and S. Yang, *J. Am. Chem. Soc.*, 2019, **141**, 19715–19727.
60 W. Liu, P. Wang, Y. Ao, J. Chen, X. Gao, B. Jia and T. Ma, *Adv. Mater.*, 2022, **34**, 2202508.
61 X. Liu, J. Pei, Z. Hu, W. Zhao, S. Liu, M.-R. Amara, K. Watanabe, T. Taniguchi, H. Zhang and Q. Xiong, *Nano Lett.*, 2020, **20**, 5359–5366.
62 M. Liu, J. Wen, R. Xiao, R. Tan, Y. Qin, J. Li, Y. Bai, M. Xi, W. Yang, Q. Fang, L. Hu, W. Gu and C. Zhu, *Nano Lett.*, 2023, **23**, 5358–5366.
63 B. He, P. Xiao, S. Wan, J. Zhang, T. Chen, L. Zhang and J. Yu, *Angew. Chem., Int. Ed.*, 2023, **62**, e202313172.
64 Y. Feng, X. Gong, S. Fan, Z. Jiang, J. Yang, Y. Qu, Y. Chen, Q. Peng, J. Ding, H. Shen, X. Qi and M. Wang, *Adv. Funct. Mater.*, 2024, **34**, 2403502.
65 Y. Mao, P. Wang and S. Zhan, *Nano Res.*, 2022, **15**, 10158–10170.
66 Z. Zhu, H. Huang, L. Liu, F. Chen, N. Tian, Y. Zhang and H. Yu, *Angew. Chem., Int. Ed.*, 2022, **61**, e202203519.
67 M. Liu, W. Yang, R. Xiao, J. Li, R. Tan, Y. Qin, Y. Bai, L. Zheng, L. Hu, W. Gu and C. Zhu, *Natl. Sci. Rev.*, 2025, **12**, nwae465.
68 Y. Xiao, J. Fu, Y. Pihosh, K. Karmakar, B. Zhang, K. Domen and Y. Li, *Chem. Soc. Rev.*, 2025, **54**, 1268–1317.
69 J. Wang, W. Liao, Y. Tan, O. Henrotte, Y. Kang, K. Liu, J. Fu, Z. Lin, L. Chai, E. Cortes and M. Liu, *Chem. Soc. Rev.*, 2025, **54**, 6553–6596.
70 Y. Zi, Y. Hu, J. Pu, M. Wang and W. Huang, *Small*, 2023, **19**, 2208274.
71 M. Peng, C. Li, Z. Wang, M. Wang, Q. Zhang, B. Xu, M. Li and D. Ma, *Chem. Rev.*, 2025, **125**, 2371–2439.
72 K. S. Exner, *ACS Catal.*, 2019, **9**, 5320–5329.
73 M. B. Gawande, K. Ariga and Y. Yamauchi, *Small*, 2021, **17**, 2101584.
74 C. Gao, J. Low, R. Long, T. Kong, J. Zhu and Y. Xiong, *Chem. Rev.*, 2020, **120**, 12175–12216.
75 W. Xu, L. Jiao, Y. Wu, L. Hu, W. Gu and C. Zhu, *Adv. Mater.*, 2021, **33**, 2005172.
76 J. Li, H. Zhang, W. Samarakoon, W. Shan, D. A. Cullen, S. Karakalos, M. Chen, D. Gu, K. L. More, G. Wang, Z. Feng, Z. Wang and G. Wu, *Angew. Chem., Int. Ed.*, 2019, **58**, 18971–18980.
77 Y. Qin, R. Tan, J. Wen, Q. Huang, H. Wang, M. Liu, J. Li, C. Wang, Y. Shen, L. Hu, W. Gu and C. Zhu, *Chem. Sci.*, 2023, **14**, 7346–7354.
78 C. Ding, J. Shi, Z. Wang and C. Li, *ACS Catal.*, 2017, **7**, 1706.
79 B. A. Nail, J. M. Fields, J. Zhao, J. Wang, M. J. Greaney, R. L. Brutchey and F. E. Osterloh, *ACS Nano*, 2015, **9**, 5135–5142.
80 Y. Chen, Y. Qin, M. Liu, W. Yang, Y. Qiu, W. Li, L. Zheng, W. Gu, C. Zhu and L. Hu, *Nat. Commun.*, 2025, **16**, 2960.
81 F. Niu, Q. Zhou, Y. Han, R. Liu, Z. Zhao, Z. Zhang and K. Hu, *ACS Catal.*, 2022, **12**, 10028–10038.
82 Y. Qin, J. Zhang, R. Tan, Z. Wu, M. Liu, J. Li, M. Xu, W. Gu, C. Zhu and L. Hu, *ACS Sens.*, 2023, **8**, 3257–3263.
83 X. Ye, X. Wang, Y. Kong, M. Dai, D. Han and Z. Liu, *Angew. Chem., Int. Ed.*, 2021, **60**, 11774–11778.
84 S. Tian, Z. Yu, Y. Wang, S. Chen, M. Li and D. Tang, *Anal. Chem.*, 2025, **97**, 9518–9526.
85 Z. Zhang, P. Sen, B. R. Adhikari, Y. Li and L. Soleymani, *Angew. Chem., Int. Ed.*, 2022, **61**, e202212496.
86 A. Clifford, J. Das, H. Yousefi, A. Mahmud, J. B. Chen and S. O. Kelley, *J. Am. Chem. Soc.*, 2021, **143**, 5281–5294.
87 S. Gu, D. Xu, J. Huang, X. Zhou, Y. Liu and Z. Zhang, *Nat. Commun.*, 2025, **16**, 4765.
88 L. G. Kahn, K. G. Harley, E. L. Siegel, Y. Zhu, P. Factor-Litvak, C. A. Porucznik, M. Klein-Fedyshin, A. E. Hipwell and Program Collaborators for Environmental Influences on Child Health Outcomes Program, *Hum. Reprod. Update*, 2021, **27**, 339–366.
89 R. Song, H. Chi, Q. Ma, D. Li, X. Wang, W. Gao, H. Wang, X. Wang, Z. Li and C. Li, *J. Am. Chem. Soc.*, 2021, **143**, 13664–13674.
90 M. G. Evich, M. J. B. Davis, J. P. McCord, B. Acrey, J. A. Awkerman, D. R. U. Knappe, A. B. Lindstrom, T. F. Speth, C. Tebes-Stevens, M. J. Strynar, Z. Wang,

E. J. Weber, W. M. Henderson and J. W. Washington, *Science*, 2022, **375**, eabg9065.
91 Y. Tang, Y. Liu, J. Wang, J. Wang and Z. Liu, *Environ. Sci. Technol.*, 2023, **57**, 2826–2836.
92 Q. Wang, M. Zhou and L. Zhang, *J. Hazard. Mater.*, 2020, **382**, 121026.
93 K. Tang and H. Zhao, *Infect. Drug Resist.*, 2023, **16**, 811–820.
94 Z. Zhang, Q. Liu, M. Zhang, F. You, N. Hao, C. Ding and K. Wang, *J. Hazard. Mater.*, 2021, **416**, 125988.
95 B. Peng, Z. Zhang, L. Tang, X. Ouyang, X. Zhu, L. Chen, X. Fan, Z. Zhou and J. Wang, *Anal. Chem.*, 2021, **93**, 9129–9138.
96 Y. Xu, Z. Wen, T. Wang, M. Zhang, C. Ding, Y. Guo, D. Jiang and K. Wang, *Biosens. Bioelectron.*, 2020, **166**, 112453.
97 X. Chen, W. Wu, J. Zeng, E. Ibañez, A. Cifuentes, J. Mao, L. Yu, H. Wu, P. Li and Z. Zhang, *J. Hazard. Mater.*, 2023, **460**, 132281.
98 Z. Xiao, Y. Chen and Y. Zhang, *Environ. Res.*, 2025, **271**, 121084.
99 H. Meng, R. Xu, K. Xu, D. Leng, L. Liu, H. Ju, X. Liu and Q. Wei, *Microchim. Acta*, 2024, **191**, 89.
100 Y. Qiao, J. Li, H. Li, H. Fang, D. Fan and W. Wang, *Biosens. Bioelectron.*, 2016, **86**, 315–320.
101 X. Meng, A. Huang, Y. Li, X. Dong and T. You, *Biosens. Bioelectron.*, 2024, **251**, 116121.
102 Z. Yu, H. Gong, J. Xu, Y. Li, Y. Zeng, X. Liu and D. Tang, *Anal. Chem.*, 2022, **94**, 3418–3426.
103 Y. Gao, M. Li, Y. Zeng, X. Liu and D. Tang, *Anal. Chem.*, 2022, **94**, 13582–13589.
104 L. Huang, G. Cai, R. Zeng, Z. Yu and D. Tang, *Anal. Chem.*, 2022, **94**, 9487–9495.
105 R. Zeng, J. Xu, L. Lu, Q. Lin, X. Huang, L. Huang, M. Li and D. Tang, *Chem. Commun.*, 2022, **58**, 7562–7565.